MICROWAVE-ASSISTED SYNTHESIS OF EUROPIUM-DOPED CALCIUM FLUORIDE NANOPARTICLES FOR POTENTIAL BIOMEDICAL APPLICATIONS

A thesis presented to the faculty of the Graduate School of Western Carolina University in partial fulfillment of the requirements for the degree of Masters of Science in Chemistry.

By

Aaron Davis Lipchak

Advisor: Dr. Channa De Silva
Associate Professor of Chemistry
Department of Chemistry & Physics

Committee Members: Dr. Scott Huffman, Chemistry & Physics
Dr. William Kwochka, Chemistry & Physics

March 2019

ACKNOWLEDGEMENTS

I would like to personally thank my friends, family, and colleagues for their support, advice, and paitence. In particular: Martin for being such a wonderful undergraduate research minion, Dr. Heather Coan for the conversation and advice about my future, Renee for all of the science puns, Paige for nicknaming me Bubbles, and Jessica for being the best long-distance friend I could ask for.

TABLE OF CONTENTS

LIST OF TABLES

LIST OF FIGURES

ABSTRACT

MICROWAVE-ASSISTED SYNTHESIS OF EUROPIUM-DOPED CALCIUM FLUORIDE NANOPARTICLES FOR POTENTIAL BIOMEDICAL APPLICATIONS

Aaron Davis Lipchak, Masters of Science in Chemistry

Western Carolina University (March 2019)

Advisor: Dr. Channa De Silva

Europium (Eu^{3+}) metal-based nanomaterials have potential applications in optical and electroluminescent devices, bio-analytical sensors, and biomedical assay technologies. Eu^{3+} metal ions are of particular interest in biological assays due to their long luminescent lifetimes and nearly monochromatic emission at 614 nm. Eu^{3+} ions require sensitization by a suitable chromophore since *4f-4f* electronic transitions are forbidden by the Laporte selection rule. Relative to well-researched lanthanide-doped matrices such as $NaYF_4$ and LaF_3, lanthanide-doped CaF_2 nanoparticles have been shown to have promise as an imaging agent due to greater luminescent yields and high biocompatibility. In this work, we report the progress towards the optimization of an aqueous microwave synthetic method for the production of nanosized lanthanide-doped CaF_2 particles, the surface-functionalization of Eu^{3+}-doped CaF_2 particles with a suitable chromophore, and luminescent quantum yield studies of these particles.

Synthesis of lanthanide-doped CaF_2 nanoparticles and the coating of them with a chromophore ligand to increase their luminescent quantum yield was successful. High-quality product may be obtained with low size dispersion anywhere in the range of 30-1000 nm. Characterization of coated nanoparticle product including the morphology, composition, and quantum yield studies were successful. The highest quantum yield reported was 1.53 +/- 0.41 %. Future work includes the optimization of the coating procedure to maximize luminescent quantum yield and in vitro imaging studies using epifluorescence microscopy.

CHAPTER ONE: INTRODUCTION

Background

Nanomaterials

Over the past few decades, nanomaterial synthesis and application have undergone a rapid increase of interest and research. In the United States, the budget for the National Nanotechnology Initiative in 2009 was 1.5 billion dollars, which was over a 300% increase since it began in 2001.[1] Nanoparticles, which are defined as particles within a size range of 1-100 nanometers, have been shown interest due to their promise in applications such as drug delivery, imaging, and targeted therapies as a replacement for chemotherapy.[2,3] At this size, particles may imitate common biological functions involved with growth and development of the human body. In particular, they may resemble common cellular proteins and DNA as they have a similar size range and may mimic the binding of proteins and DNA to cell receptors. Nanoparticles that can be used in biomedicine must be non-toxic, water-dispersible, and relatively easy to produce. Development of synthetic methods for the production of nanoparticles that allow for the precise control of shape, size, composition, surface modification, and other characteristics form the basis for research in this field.[1] As interest in the field of nanomedicine continues to grow, the need for methods that fulfill all of these criteria are required. They have so far been proven rare, with oftentimes only most of the criteria being met.

Many biomedical applications of nanoparticles involve the functionalization of the surface of the particles with a chemical known to bind to a specific cell receptor. Such a system allows for the direct targeting of specific cells and cell types of interest. The patient may be scanned after administration to look for areas of high concentrations of nanoparticles, signifying areas where cells or cell types are present, using detection methods for luminescence or magnetism depending on the intrinsic characteristics of the particles. Luminescence is of particular interest to biomedical researchers due to the convenience of detecting very small amounts of light by the

usage of extremely sensitive devices such as photodetectors.

For example, researchers at the Chinese Academy of Sciences in Xiamen, China produced a $Zn_{1.1}Ga_{1.8}Ge_{0.1}O_4:Cr^{3+}/Eu^{3+}@SiO_2$ shell:core product for use in tumor imaging. Folic acid, known to be a tumor-targeting group, was used to functionalize the surface of the particles. Both *in vitro* and *in vivo* imaging was completed with success. These results showed that their luminescent nanoprobe system was capable of accurately targeting tumors and can be used to track in real-time progress of the drug delivery.[4]

Past Research Concerning Lanthanide-Based Luminescent Nanoparticles

Nanoparticle systems doped with lanthanides have shown great promise as luminescent probes in biomedicine for many reasons. Common organic luminescent dyes undergo photobleaching that diminishes their luminescent efficiency (defined as the number of photons emitted over the number of photons absorbed), reducing the timespan in which imaging systems using dyes may effectively operate when compared to lanthanide-based systems which do not photobleach appreciably. Organic dyes also have broad emission peaks which are troublesome due to the high amount of background sample autofluorescence. The large amount of background signal in biological samples limits the sensitivity of the measurements. On the other hand, lanthanide-based materials emit well-defined and narrow emission peaks when compared to organic dyes and biological materials, allowing their signal to be easily distinguished from background noise. Figure 1 shows the emission spectra comparing a common organic dye, cresyl violet, to the emission of europium(III).

The long luminescent lifetimes of lanthanides relative to organic dyes and tissue also provide an advantage in separating analyte signal from background signal through the usage of time-gated signal acquisition, allowing for a higher signal-to-noise ratio.[5] Lanthanide ions also undergo a large Stokes-shift, which is the difference in the band peaks between the excitation and emission signal. Having a large Stokes-shift allows analyte signal to be better distinguished from biological autofluroescence as the latter is typically closer to the UV end of the visible spectrum.

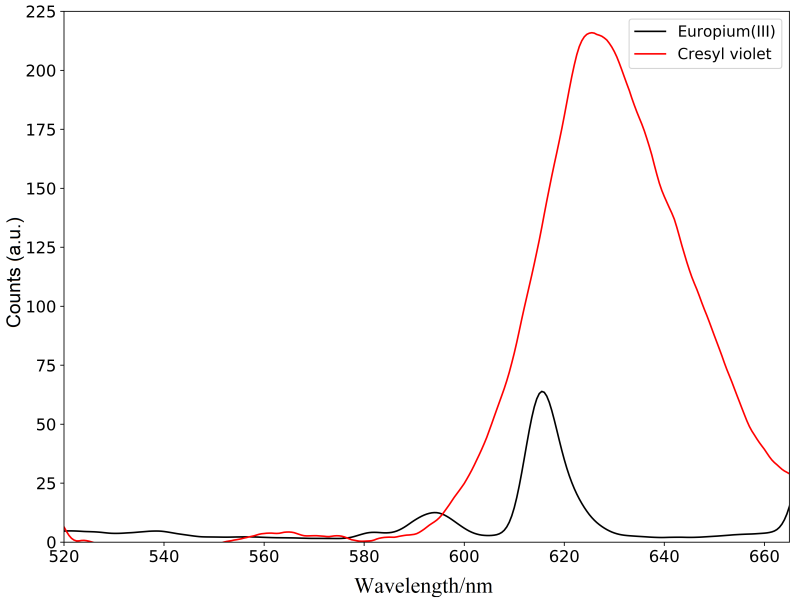

Figure 1. Emission spectra of cresyl violet, an organic dye, and europium(III), a lanthanide element.

Pure lanthanide compounds, such as LaF_3, are inefficient due to self-quenching of lanthanide ions. This self-quenching is the result of the close proximity of ions canceling out each other's electronic transitions. Crystal matricies that allow for the controlled doping of lanthanide ions into them are used as this provides space between the ions to prevent this phenomena. Previous lanthanide-based nanoparticle matrices that have been well researched include $NaYF_4$ and LaF_3. Er^{3+} and Yb^{3+} have been doped into the $NaYF_4$ matrix with absolute luminescent quantum yields of 0.005 to 0.3 %.[6] Another interesting result found by Boyer et. al. was a 95 % decrease in quantum yield when the average nanoparticle size was reduced from 30 to 10 nm.[6] LaF_3 has been doped with lanthanides to greater success, with LaF_3: Ce^{3+} 10 %, Gd^{3+} 30 %, Eu^{3+} 1 % nanoparticles reported to have absolute quantum yields between 4 and 16 % using different surfactants. Surfactants such as polyacrylic acid (PAA), ethylaminediaminetetraacetic acid (EDTA), citric acid, and olelyamine were found to significantly influence the size and morphology of the

nanoparticle product. In this codoped fluoride product, it was reported that the charge transfer transition states between Ce^{3+}, Gd^{3+}, and Eu^{3+} allowed for the relatively efficient red emission from Eu^{3+}.[7]

The primary issue with current lanthanide-based nanoprobes are low luminescent yields, causing them to be difficult to detect *in vivo* due to a low signal-to-noise ratio. Causes of these low luminescent yields are innate to lanthanide (Ln) ions. Firstly, aqueous solutions containing Ln ions lead to significant quenching (any non-radiative relaxation of excited states) due to O-H vibrational interactions. Secondly and most importantly, the shielding of the *4f* orbitals in Ln ions by the filled 6s and 5p sub-shells causes Ln ions to have very low molar absorption coefficients due to LaPorte parity-forbidden *4f-4f* electronic transitions.[8]

Paths to minimize these effects are of special importance in Ln based nanoprobes. To overcome the LaPorte selection rule, chemicals commonly called chromophores are used. Chromophores form complexes with Ln ions and allow the efficient absorption of light and transfer of that energy to the excited state of the Ln ion through ligand-to-metal charge transfer (CT) transition states, circumventing the forbidden *4f-4f* electronic transitions. Good chromophores for Ln ions need to have high molar absorption coefficients and a high degree of conjugation in order to transfer the energy to Ln ions through π to π^* transitions. In the case of thenoyltrifluoroacetone (TTA) which will be described later, light is absorbed via a singlet state electronic excitation (S_0 - S_1). Energy is then transferred to a triplet state within TTA (S_1 - T_3), and finally a ligand to metal energy trasnfer process to populate the excited state (D) within the Ln ion which may undergo luminescence in a relaxation to a ground state (F).[8]

Past Research Concerning Lanthanide-Doped Calcium Fluoride

Calcium fluoride poses a few advantages as a matrix for lanthanide-doped nanomaterials. Known to be transparent from the UV through the visible to mid-IR electromagnetic regions, it has been used in applications such as optical lenses where far-UV transparency is desired.[9] Calcium ions also have a similar radii to most lanthanide ions, allowing the well-studied cubic fluo-

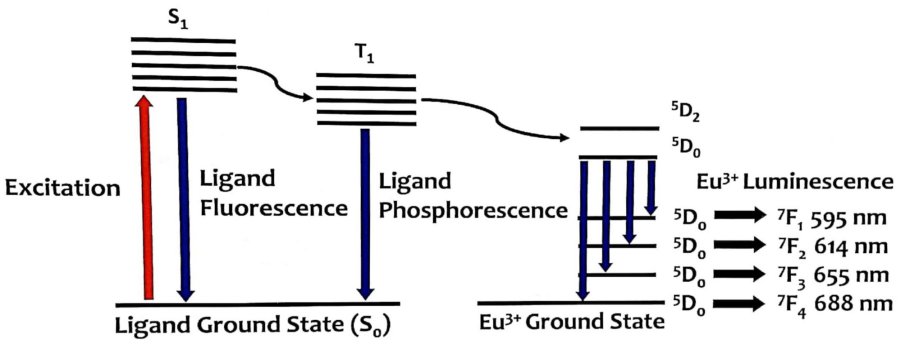

Figure 2. Ligand-to-metal charge transfer process of Europium complexes.

rite crystal structure of CaF_2 to be easily doped with lanthanide ions. CaF_2 is known to be highly biocompatible, with fluoride compounds being added to dental products to promote the formation of CaF_2 on teeth, as well as being very tolerant of extreme physiological conditions owing to it's high chemical stability.[9]

Due to the high reaction rate constant for the formation of CaF_2 when ionized Ca^{2+} and F^- are present in solution, various methods have been found to create nanomaterials. A double-jet precipitation synthesis originally used to produce LaF_3 was adapted for the production of CaF_2.[10] In this synthesis, two solutions, one of calcium nitrate and another of sodium fluoride, were simultaneously added dropwise under vigourous stirring to a heated solution. This allowed for the fine control of concentrations inside of the reaction solution. This method produced cubic nanocrystals with an average size of 9-180 nm depending on conditions.

Few articles have been published reporting the quantum yields of lanthanide-doped calcium fluoride nanoparticle product. Of those few, some under-report the methods used for the determination of quantum yields. Those with sufficient reports of the methods used to determine quantum yields are as follows:

Eu^{3+}-doped CaF_2 nanoparticles coated with salicylic acid were produced through a precipitation method.[11] A solution of $CaCl_2$ and $EuCl_3$ in methanol was prepared and added dropwise to a solution containing NH_4F in methanol. The presence of salicylic acid was found to increase

the luminescent activity, though no quantum yield measurements are completed on this product. A similar approach was used using ethanol solutions in place of methanol. They did not coat the nanoparticle product with a surfactant, but they found that the luminescent activity of Eu^{3+}-doped CaF_2 product reached a maximum at around 15% mol Eu^{3+} concentration.[12] Again, quantum yield measurements were not completed in this study.

Lanthanide-doped calcium fluoride has already been applied to a few aspects of biomedicine, including stem cell labeling and timed drug-release therapies. A $NaYbF_4$:Tm^{3+}/CaF_2 core/shell product functionalized with polyethylenimine (PEI) and used for targeting rat mesenchymal stem cells (rMSCs) with great success.[13] Zhang et. al. developed hollow spheres (300-930 nm in diameter) comprised of Ce^{3+}/Tb^{3+} codoped CaF_2 nanocrystals about 40 nm in size.[14] The highest quantum yield they reported with this material was 77%. They also showed this system's potential as a drug carrier, using ibuprofen as a model, by succeeding in tracking the release of ibuprofen through changes in the green emission of Tb^{3+}.

Introduction to Project

First, a microwave-based method of producing monodispersed Eu-doped CaF_2 nanoparticles must be optimized. This method has previously only been used to dope terbium and cerium into the CaF_2 crystal matrix. Second, the surface of the nanoparticle product will be functionalized with TTA (thenoyltrifluoroacetone) to increase the luminescent quantum yield. Both the surface-functionalization of $EuCaF_3$ product with TTA chromophore, and the optimization of the microwave-based method to produce nanoparticles are novel research in this project. In addition, the luminescent quantum yield is not well-established for nano-sized lanthanide-doped calcium fluoride materials, so this work will fill a neccessary gap in the research regarding these materials.

Characterizations will be performed, with the most important being the luminescent quantum yield studies to ascertain the effect of TTA. Morphology and composition studies will also be performed. To attempt to improve the quantum yield (ϕ) of lanthanide-doped calcium fluo-

ride nanomaterials, the surface of europium-doped CaF_2 nanoparticles will be functionalized with TTA, which is known to have efficient electronic transitions with Eu^{3+} ions as described in Figure 2.[15] $Eu[TTA]_3[H_2O]_2$ complexes will also be produced for comparison purposes.

Project Design

Aqueous Microwave-Enhanced Co-Precipitation

In 2013, Lin Ma *et al.* reported an aqueous microwave-enhanced co-precipitation method for the production of monodispersed calcium fluoride (CaF_2) microspheres.[16] In order to overcome the quick reaction rate towards CaF_2 which has historically been an obstacle in the production of high quality nanomaterials, it was theorized that the decomposition of chelated Ca^{2+} ions under microwave irradiation and the usage of sodium tetrafluoroborate ($NaBF_4$) as a F^- ion source would allow for better control of the reaction rate. A chemical equation for this synthesis is shown in Figure 3.

$$Ca^{2+}_{(aq)} + Eu^{3+}_{(aq)} + EDTA_{(aq)} + F^-_{(aq)} \xrightarrow[H_2O,\ pH\ 6]{\text{Reflux in microwave}} Eu{:}CaF_{2\,(s)}$$

EDTA-coated particles

Figure 3. Chemical equation for the microwave-assisted synthesis of Eu^{3+}-doped CaF_2 nanoparticles.

The chelating agent used was ethylaminediaminetetraacetic acid (EDTA, Figure 4), which is very well known in industry and medicine for being a strong chelating agent towards divalent and trivalent positive ions. Under reflux in an aqueous solution, EDTA complexes are not well known to appreciably release bound cations. Lin Ma *et al.* theorized that microwave irradiation, commonly thought to quicken reaction rates by either directly intefering with and overcoming reaction intermediates or by increasing the microscopic temperature of the reaction chamber, would

provide a controlled influx of cations through decomposition of EDTA complexes.[16,17] Another potential advantage of using microwave irradiation for the heating of reaction chambers includes the relatively homogeneous heating gradient relative to conventional heating methods, which is essential for producing homogeneous products and providing an easily scalable platform for industry.[17]

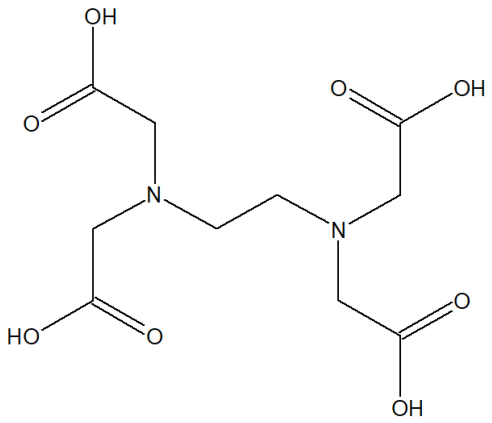

Figure 4. Chemical structure of ethylenediaminetetraacetic acid (EDTA).

The CaF_2 product that Lin Ma *et al.* reported was about 1.1 μm when undoped, while cerium/terbium-doped CaF_2 (theoretical 10% dopant) was slightly smaller at about 1.0 μm. It was suggested that the smaller size may be due to the slower decomposition of trivalent lanthanide[EDTA] complexes relative to divalent Ca[EDTA] complexes under microwave irradiation.[16]

In order to optimize the method to produce smaller particles, a path outlined by Williamson *et al.* was explored.[18] They found that increased overall concentrations of reactants led to a decrease in the size of particles and improvement in size dispersion in a model synthesis. Repeating these results with the previously mentioned CaF_2 method was explored. A goal of 50 nm was set, as this size particle was shown to have the greatest intake in mammalian cell lines.[19]

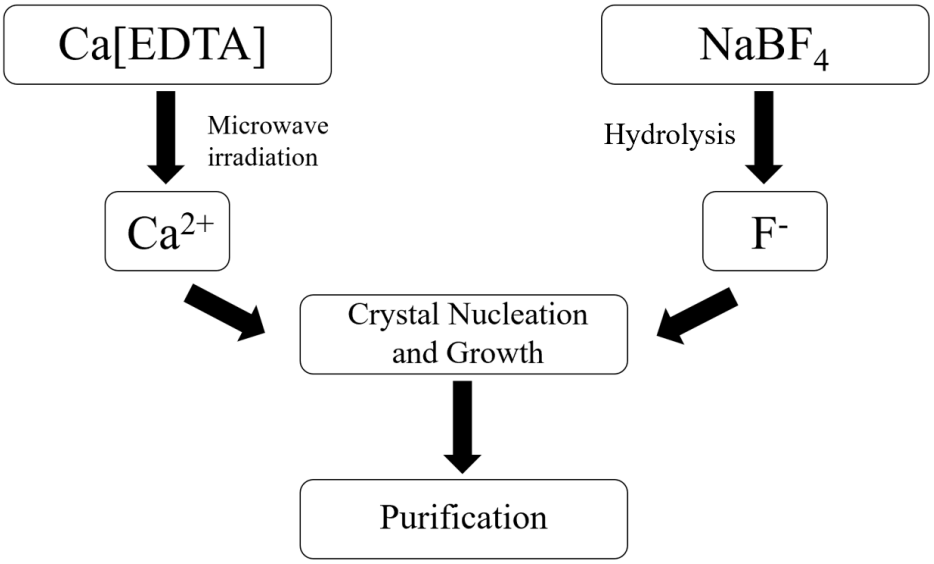

Figure 5. Microwave-enhanced co-precipitation reaction diagram for calcium fluoride.

Coating Particle Surface with a Chromophore

Since the above method uses an excess of EDTA in order to control the influx of cations in the reaction, it is safe to assume that the resultant product will be coated with EDTA. A ligand exchange of EDTA with thenoyltrifluoroacetone (TTA, Figure 6), which is solubilized and de-protonated using the base triethylamine, was performed in water. Triethylamine is also present to create enolate ions, which have an afinity for lanthanide ions. This mechanism is shown in Figure 7. The enolate TTA ion forming a ligand with a lanthanide ion is shown in Figure 8.

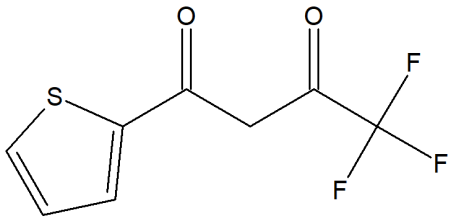

Figure 6. Chemical structure of thenoyltrifluoroacetone (TTA).

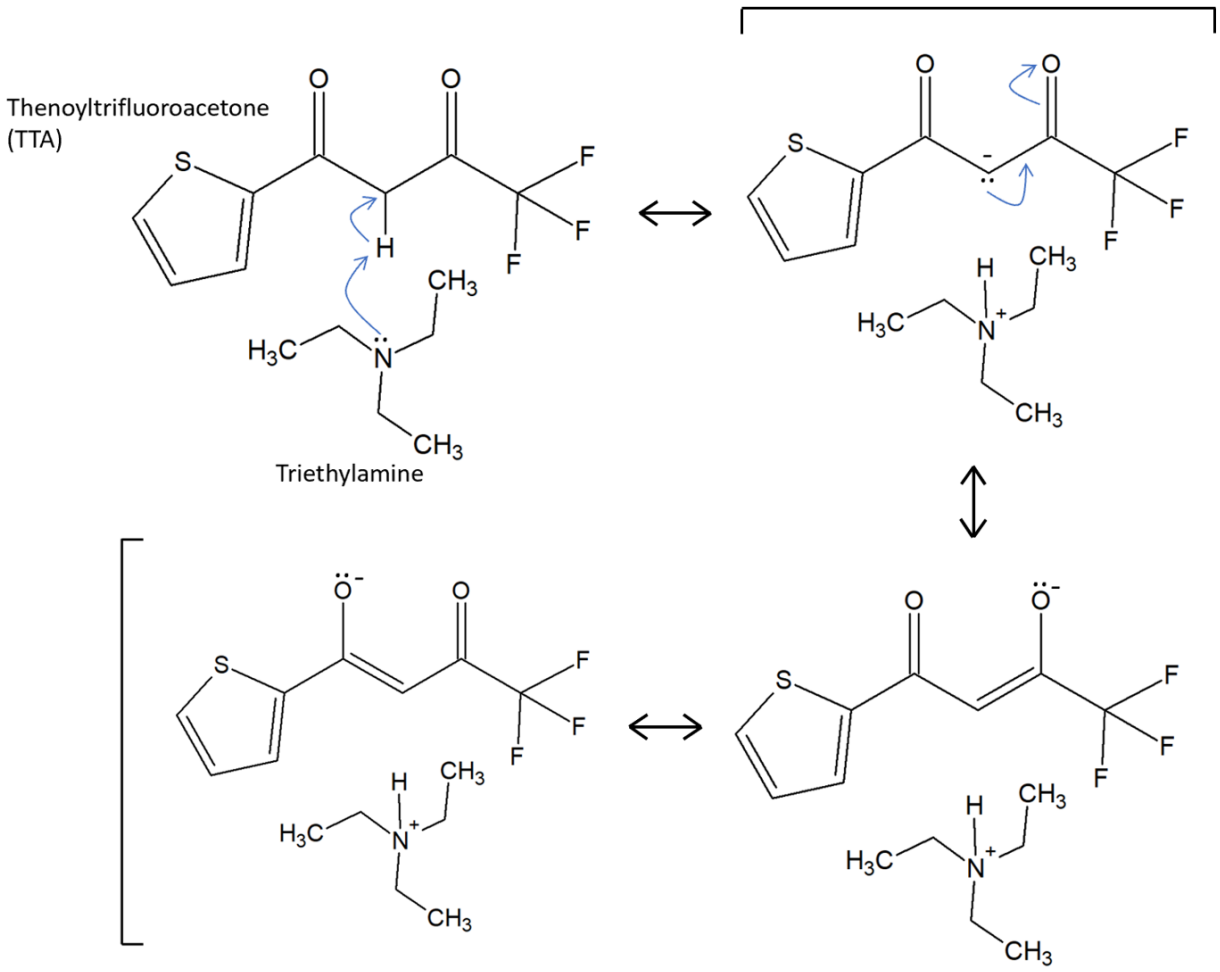

Figure 7. Reaction mechanism of thenoyltrifluoroacetone (TTA) and triethylamine forming an enolate to increase binding affinity to Lanthanide ions.

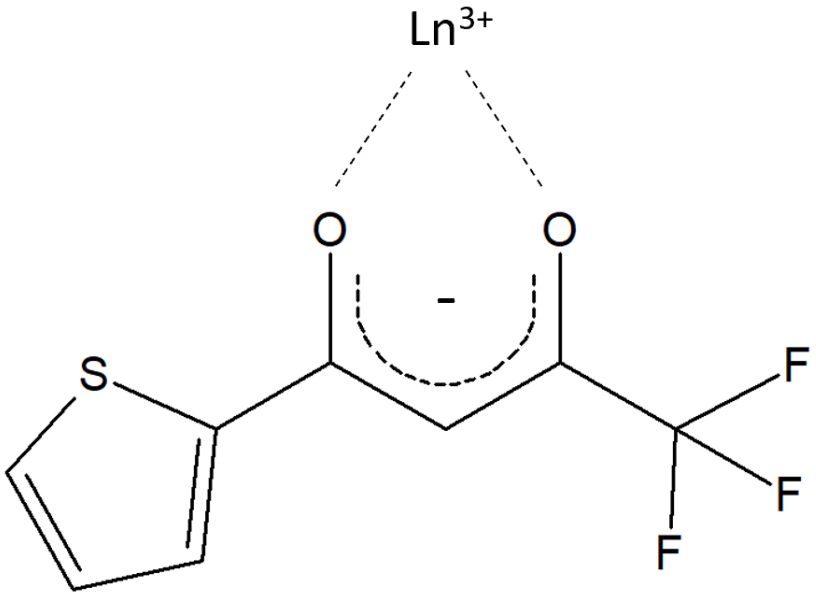

Figure 8. The enolate TTA ion binding to a lanthanide ion to form a metal ligand.

CHAPTER TWO: EXPERIMENTAL

Synthesis

Materials

All materials and reagents were used without further purification. All water used in all syntheses was ultrapure grade. All glassware used was first washed with 5% nitric acid solution, followed by 10 g/L Alconox detergent solution, and finally rinsed with water. All pH measurements were taken using a Vernier pH sensor connected through a GoLink adaptor to a computer via USB. Logger Lite software, supplied by Vernier, was used to read and take pH measurements. All sonication was performed in a Fisher Scientific Ultrasonic Bath, and all centrifuge tubes were polyethylene produced by Falcon Corning brand. Reagents are as follows: $CaCl_2$.anhydrous (Fischer Scientific, 10043-52-4), $EuCl_3.6H_2O$ (Strem Chemicals, 13759-92-7), ethylenediaminetetraacetic acid (Fischer Scientific, 6381-92-6), sodium tetrafluoroborate-old sample (Alfa Aesar, 13755-29-8), sodium tetrafluoroborate-new sample (Acros Organics, 13755-29-8), thenoyltrifluoroacetone (Aldrich), and triethylamine (Mallinckrodt, 121-44-8).

Microwave-Assisted Synthesis of Lanthanide-Doped Calcium Fluoride Nanoparticles

A CEM Discover 300W microwave instrument was used for all syntheses, operated by Synergy software.

In a typical synthesis for doped CaF_2 nanoparticle product with an average size of about 50-60 nm, a solution containing $CaCl_2/EuCl_3.6H_2O$/EDTA (5.2 total mmol of metal chlorides) (2.72 g 2NaEDTA or 6.4 mmol EDTA) was prepared in ultrapure water (55 mL) under sonication and adjusted to a pH of 6.0 using 4.0 M NaOH solution. $NaBF_4$ (1.14 g, 10.4 mmol) was dissolved in water (20 mL) under sonication, added dropwise to the previous solution, and readjusted to pH 6.0 using 4.0 M NaOH solution. The reaction solution was left to stir for 5 minutes, then transferred to a 100 mL roundbottom flask for final concentrations of 0.065/0.08125/0.13M (metal chlorides/EDTA/$NaBF_4$) with an estimated total volume of 80 mL (accounting for the 5

mL headroom for any added NaOH solution to adjust the pH).

The flask was transferred to a microwave reaction instrument with both an air condensing tube and cold water condensing tube attached. Due to a 100 mL roundbottom flask being the largest flask that may be used in the microwave instrument and the reaction solution being 80 mL, the air condenser was primarily to have space for the boiling reaction to expand. The setup is shown in Figure 9.

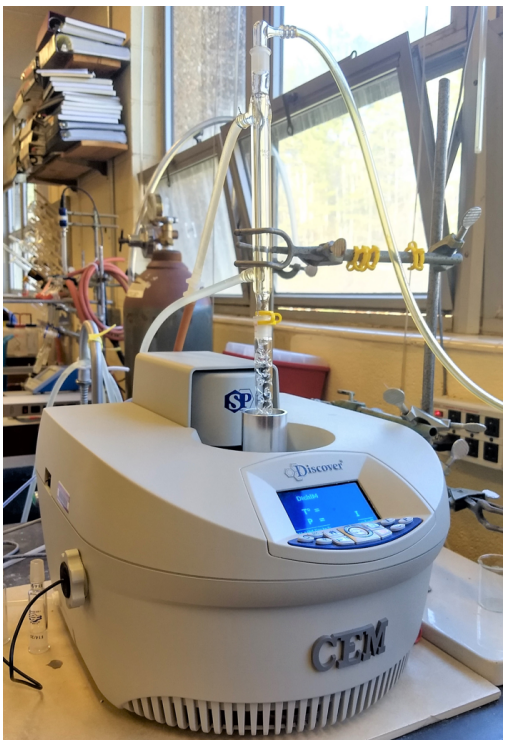

Figure 9. Microwave instrument setup for the synthesis of lanthanide-doped calcium fluoride particles.

The software was set to operate the reaction at a constant power of 100 Watts for 30 minutes. Beginning at room temperature, the reaction heats up to reflux (100 °C) after 5 minutes. This temperature is held for the remainder of the synthesis. After the reaction was completed, the flask was allowed to cool through convection for 5 minutes, then transferred to a freezer to cool

to room temperature. A preliminary size distribution may be gathered from DLS instrumentation at this point. Once cooled, the reaction solution was transferred to two 50 mL conical centrifuge tubes and centrifuged once for 10 minutes at 2500 rpm to separate large particles and impurities. The solution was decanted to a new set of conical tubes, then centrifuged for 4 hours in a Sorvall RC 5C Plus centrifuge (equipped with an HS-4 rotor) 3 times at 6000 rpm to remove dissolved impurities, the waste solution decanted, the product redispersed in 15 mL of water, and finally transferred to new conical tubes to minimize risk of damage to the tubes. A UV lamp set to 325 nm was used to ascertain that the collected product at the bottom of each tube was luminescent, indicating that it contained europium ions. After the third centrifugation, the product was redispersed in 10 mL of ethanol and dried in a rotovap system. If the product did not appear completely dry, it was left to dry overnight covered with a Kimwipe in a fume hood at room temperature.

After each synthesis, the reaction vessel was rinsed with 5% nitric acid solution to remove build-up of CaF_2 on the inside surface of the flask. This was done after noticing the build-up of a white film up to the level of the solvent after multiple syntheses. Alconox cleaning solution was not sufficient in removing this.

Traditionally Heated Synthesis of Europium(III)-Doped Calcium Fluoride Particles

For comparison purposes, the microwave-assisted synthesis was replicated using a traditional heating method. All other method parameters were identical to the microwave-assisted method. A heating mantle connected to a transformer to adjust voltage was used. The transformer was set to 100% during the temperature ramping stage, then dialed back to 50% during reflux. This setup is shown in Figure 10.

Synthesis of $Eu[TTA]_3[H_2O]_2$ Complex

For comparison to TTA-coated Eu^{3+}-doped CaF_2 nanoparticle product, $Eu[TTA]_3[H_2O]_2$ complex was synthesized. Three molar equivalents of TTA (thenoyltrifluoroacetone) (0.333g, 1.5 mmol) was dissolved in ultrapure water (10 mL) with a minimum amount of concentrated (2.0-

Figure 10. Heating mantle setup for the synthesis of europium(III)-doped calcium fluoride nanoparticles.

4.0 M) NaOH solution and was heated to 60 °C. One molar equilvalent of $EuCl_3.6H_2O$ (0.183 g, 0.5 mmol) was dissolved in 10 mL of water and heated to 50 °C. The TTA solution was added dropwise to the $EuCl_3.6H_2O$ solution under constant stirring, and a white precipitate was formed. This solution was held at 50 °C while stirring for 30 minutes , then cooled to room temperature for 2.5 hours under stirring. The solution with white precipitate was filtered under vacuum, using 20 individual 1 mL portions of water to rinse and finally 1 mL of ethyl ether to aide in drying the product. The filter paper with the product was allowed to dry overnight at room temperature.

TTA Coating Using Varying Concentrations

Thenoyltrifluoroacetone (TTA) ligand exchange on the surface of the nanoparticle product was completed as follows. Only one concentration of TTA coating was performed, as time allowed. 50 mg of TTA was measured and added to ultrapure water (3 mL). To this solution, a minimal amount of triethylamine was added to solubilize the TTA in water. For 50 mg of TTA,

150 uL of triethylamine was used. Sonication was used to aid in the solubilization of TTA in water. Another solution was prepared by mixing nanoparticle product (40 mg) in ultrapure water (7 mL), sonicating for two minutes to ensure dispersion. The solutions (one of 50 mg of TTA in 3 mL water with triethylamine and one of 40 mg of nanoparticle product in 7 mL water) were combined in a 50 mL conical centrifuge tube and shaken for one hour using a Burrell Wrist Action Shaker.

To purify, the mixture was centrifuged at 5000 rpm for 8 minutes and decanted. Product was redispersed in 10 mL of water, and centrifuged again. This process was repeated once more using 95% ethanol. Conical centrifuge tubes were placed in a hood to dry overnight at room temperature.

Characterizations

Powder X-Ray Diffractometry

Powder X-ray diffractometry (P-XRD) was used to determine the crystalline purity of the powdered product. A Rigaku Miniflex XRD instrument paired with Jade 7 software was used. The product was applied to an XRD plate and scanned within the range of 15 to 85 2θ at a rate of 0.01 2θ per second. XRD plates were prepared by making a concentrated slurry of nanoparticle product with ethanol which were transferred to the plate a few drops at a time, and allowed to dry. The product was applied until an even coating of the nanoparticle product formed on the entire surface of the plate.

P-XRD will also be used to estimate the average crystallite size using the Scherrer equation:

$$D = \frac{\lambda}{\beta cos\theta} \tag{1}$$

where D is the average crystallite diameter, λ is the X-Ray wavelength (1.5418 Å for the instru-

ment used), β is the full width at half-maximum for a chosen peak in radians, and θ is the angle corresponding to that peak in radians.[20] In general, the broader the peak, the smaller the crystallite size. Assuming that no other factors are attributing to band broadening, the Scherrer equation may provide an accurate estimate for nano-sized crystallites. There are many other factors that influence band broadening, primarily due to crystalline imperfections and impurities that will cause the Scherrer equation to yield estimates of smaller-than-actual particle size.[21] If these are present, such as when Eu^{3+} is doped into the CaF_2 crystal matrix, the Scherrer equation will yield less accurate estimations of particle size. There are important distinctions between crystallite size, grain, and particle size. Particles are composed of multiple grains, which are independently diffracting entities with identifiable boundaries. In literature, grains and crystallites are synonymous with each other unless grains contain many imperfections. If imperfections are present, grains are considered to be comprised of multiple crystallites.

Since the instrument uses a cobalt X-ray source, and the standard for reporting in chemistry journals is a copper source, Jade 7 software was used to convert the data from cobalt to copper source. Jade was also used to calculate the full width at half maximum (FWHM) values for use in the Scherrer equation.

Dynamic Light Scattering

A preliminary qualitative measurement for the size distribution of the product was performed using dynamic light scattering (DLS) instrumentation. This technique estimates the size distribution of particles suspended in solution based on how light refracts through them. A Malvern Zetasizer instrument was used to perform these measurements. Significant difference (+25%) in the average size is expected as compared to electron microscopy images due to solvent effects. The software uses a Polydispersity Index (PDI) to describe the size dispersion of samples. A PDI value of 0.05 or less indicates high-quality samples, while lower-quality samples is indicated the closer to 1.0 the PDI value is.

In a typical synthesis, 2-3 mg of EDTA-coated nanoparticle product and 1 mL of water was

placed into a disposable plastic cuvette. This cuvette was sonicated for 30-60 seconds to disperse the product before being analyzed. For TTA-coated samples, an equivalent amount of product was dispersed in either methanol or 1:1 methanol:water mixture depending on quality of data. Different solvent mixtures yield different dispersion in solution. For EDTA-coated samples, the instrument was set for using water as a dispersant, with the temperature set to 25.0 °C, viscosity to 0.8872 cP, and refractive index for the dispersant set to 1.330. The refractive index for CaF_2 was set to 1.433. If an organic solvent was used, the method was changed to reflect the refractive index of the dispersant and glass cuvettes were used. All of these values were presets within the software.

Fourier-Transform Infrared Spectroscopy

Fourier-transform infrared spectroscopy (FT-IR) was performed to quantify the coating of nanoparticle product with TTA by observing spectra for a decrease in characteristic peaks for EDTA and an increase in characteristic peaks for TTA. FT-IR was also performed to identify what surfactants were present after synthesis, and the identification of any potential changes in spectra when comparing neat compounds with those bound to the surface of nanoparticles.

A Thermo Scientific Nicolet iS10 with a Smart iTX accessory with diamond crystal was used for FT-IR measurements. Each measurement was of 64 coherently added scans with a resolution of 1.0 and data spacing of 0.121 cm^{-1}.

UV-Visible Absorption Spectroscopy

UV-visible absorption spectroscopy (UV-Vis) was used to determine the maximum absorbance wavelength of the primary absorption peak of TTA-coated Eu^{3+}-doped CaF_2 nanoparticles for use in quantum yield measurements. Absorbance studies were also used to qualitatively monitor the TTA coating. Due to the diagnostic absorbance peak at 340 nm, the relative success of EDTA to TTA ligand exchanges at varying concentrations was extrapolated.

An Agilent Cary Series UV-Vis-NIR spectrophotometer was used for the absorbance studies. The instrument was allowed to warm up for 45 minutes before measurements. Samples were

scanned between 800 and 200 nm at a scan rate of 600 nm/min and data interval of 1 nm.

In a typical measurement, 2-3 mg of nanoparticles were placed in a plastic disposable cuvette followed by 3 mL of an appropriate solvent (water or methanol) for dispersion. This cuvette was sonicated for 30-60 seconds before it's contents were transferred to a four-sided quartz cuvette. This transfer is to ensure that the maximum amount of signal being measured is from nanoparticles and not from aggregations. The sample was diluted in the cuvette until the absorption at 340 nm was between 0.4 and 0.6.

For preparation of the reference sample for quantum yield measurements, a very small amount of cresyl violet acetate (1 mg) was dissolved in 1 mL of methanol. This solution was added dropwise to a four-sided quartz cuvette containing methanol until absorption at 317 nm was around 0.05 to 0.15.

Fluorometry

The same samples that were prepared for UV-Vis spectroscopy quantum yield measurements was used for luminescent measurements. A Perkin Elmer LS 55 Luminescence Spectrometer was used for luminescent studies. For emission studies, the sample was excited at 340 nm and scanned from 520 to 700 nm at a rate of 200 nm/minute. The excitation and emission slit widths were set to 5 nm. Cresyl violet acetate was used as a reference material for quantum yield calculations (ϕ = 0.54). Cresyl violet was excited at 317 nm. This was chosen because it is the wavelength at absorption maximum (λ_{max}) of a peak that is in the same area of the UV range as that of the Eu[TTA] wavelength at absorption maximum.

In excitation studies, the emission wavelength was held constant while the excitation wavelength was scanned. This is performed to make sure the maximum emission wavelength is selected for quantum yield measurements. The exciation scan is performed over the entire UV range, within which TTA has it's (λ_{max}). Assuring that this λ_{max} yields the greatest amount of emission validates why this excitation wavelength is selected for quantum yield studies.

Quantum Yield

Due to the difficulties of accurately and directly measuring the quantum yield of a sample by counting all photons undergoing luminescence, as an expensive integrating sphere is required, an indirect method is used. This method compares various data from a sample and a reference material to estimate the luminescent efficiency (quantum yield) of the sample. A compound whose quantum yield is well established was used as a reference material and various data from both the sample and reference will be ratioed together in order to calculate the quantum yield of the sample:

$$\phi_s = \phi_r \frac{Abs_r}{Abs_s} \frac{A_s}{A_r} \frac{n_s^2}{n_r^2} \tag{2}$$

where Abs is the absorbance at 340 nm for the sample and at 317 nm for the reference, A is the integrated area under the emission curve, and n^2 is the squared refractive index. Subscripts r and s are reference and sample, respectively.[22]

Cresyl violet (ϕ = 0.54 in methanol) is used as the reference compound when calculating the quantum yield of $EuCaF_3$ nanoparticles.[23,24] Due to the quenching of luminescence in aqeuous solutions, quantum yield measurements for TTA-coated $EuCaF_3$ samples were performed in an organic solvent, methanol. This quenching is due to the vibrational bands of the O-H bond in water molecules absorbing energy from the excited state of lanthanide ions.[25]

All samples were measured a total of nine times, or three times each on three separate days. If multiple samples were analyzed in one time frame, they were staggered each day (Day 1-ABC, Day 2-BCA, Day 3-CAB). This was done to take into account the inconsistencies of the highly sensitive fluorometric spectrometer. Slight changes in lamp temperature or voltage can result in significant changes in signal. In order to minimize the effects of evaporation, product settling, and product aggregation, the nanoparticles and cresyl violet reference were measured in quick

succession until three measurements each for absorption and luminescent emission were completed for each respective day.

Scanning/Transmission Electron Microscopy and Energy-Dispersive X-ray Spectroscopy

The morphology and the average size of the nanoparticles were determined by transmission electron microscopy (TEM). A quantitative average size of the particles was determined by manually measuring 100 particles using the reference ruler included in electron microscopy images and averaging this data.

Energy-dispersive X-ray spectroscopy (EDX) was used to determine the elemental composition of the Eu^{3+}-doped CaF_2 nanoparticles.

Due to Western Carolina University not possessing an electron microscope nor an EDX, the instrumentation at Clemson University was used for imagery and compositional studies. The Hitachi H-9500 TEM instrument is shown in Figure 11, the Hitachi HD-2000 instrument used for EDX measurements is shown in Figure 12.

Inductively Coupled Plasma - Optical Emission Spectroscopy

The actual percent composition of cations in each product was determined in triplicate using inductively coupled plasma - optical emission spectroscopy (ICP-OES). The relative concentrations in each % doped sample will be analyzed and used to determine the actual % composition of Eu^{3+} doped into the CaF_2 nanoparticle samples. Due to the difference in binding affinty of EDTA to calcium and europium ions, significant differences between the actual and theoretical percent yield was expected.[26] Since concentrated NaOH solution was used to adjust the pH of the reaction mixture, Na^+ will be analyzed alongside Ca^{2+} and Eu^{3+}. NaF is very soluble in water relative to CaF_2 and EuF_3, so it is not expected to be incorporated into the crystal matrix of the nanoparticle product.

A Perkin Elmer Optima 4100 DV was used for ICP-OES measurements. For the method, the plasma gas flow was set to 15, auxillary to 0.2, and nebulizer to 0.8 L/min. The RF power was set to 1300 watts, and the pump flow rate to 1.50 mL/min. Each measurement was the average of

Figure 11. Hitachi H-9500 TEM at Clemson University.

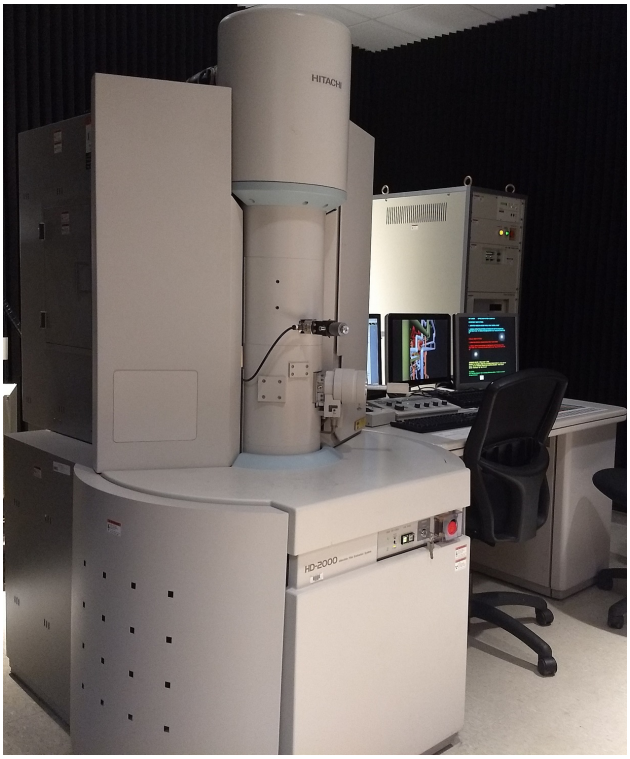

Figure 12. Hitachi HD-2000 SEM/EDX at Clemson University.

3 readings, and a 60 second rinse time was set between each standard or sample. The 393.048 nm spectral line was used for europium, while the 317.933 nm spectral line was used for calcium.

A calibration curve for calcium and europium ions was created using 6 known standards on a range of about 0.1 ppm to 2.5 ppm. 66.4 mg of $CaCl_2.2H_2O$ and 69.7 mg of $EuCl_3.6H_2O$ were placed into a 250 mL volumetric flask, using water to dissolve, yielding a concentration of about 250 ppm of each ion. From this standard, a micropipette was used to transfer a volume to a 50 mL volumetric flask, which was filled with 5% nitric acid. Exact concentrations of each ion in each standard are listed in Table 1.

Each percent Eu^{3+} doped sample (2.5, 5, 10, 15, 20, 35), as well as a 20% doped sample produced using a heating mantle, was analyzed in triplicate. A digestion method used for alkaline earth fluorides was adapted using a combination of boric acid and nitric acid. With it, alkaline earth fluorides are decomposed into soluble HBF_4 salts and BF_3 gas.[27] For preparation of Eu^{3+}-

doped CaF_2 samples, about 5 mg of nanoparticle product was weighed and placed into a 50 mL volumetric flask. To digest the sample, 2 mL of concentrated (0.64 M, 4 g/0.1 L) boric acid and 2 mL of concentrated (70%) nitric acid were added and heated for 60 seconds on a hotplate. The volumetric flask was filled to the mark with water, creating a sample of 50 ppm. Of this sample, 1 mL was diluted in another 50 mL volumetric flask for a final concentration of about 1 ppm.

For the determination of the actual percent concentration of Eu^{3+} ions in each sample, the percent composition of each respective element in regards to the total was calculated using the method of least-squares analysis.

Table 1. Actual concentrations of ICP-OES standards.

Ion	**Std 1/ppm**	**Std 2/ppm**	**Std 3/ppm**	**Std 4/ppm**	**Std 5/ppm**	**Std 6/ppm**
Europium(III)	0.279	0.558	1.115	1.673	2.230	2.788
Calcium(II)	0.106	0.213	0.425	0.637	1.062	2.125

Chemometrics

The Python programming language, using the open-source Jupyter interface, was used for chemometric purposes. Those purposes include: background correction of Eu^{3+} emission to eliminate the interference of 2^{nd}-order diffraction during integration, baseline correction of cresyl violet emission, and integration of emission spectra using a trapezoidal integration method, and smoothing of XRD spectra. For the smooting of XRD spectra, a simple convolution function was used.[28]

For the background correction of Eu^{3+} emission, a 4th-order polynomial was generated using the polyfit function in the numpy module. An example of this background correction is shown in Figure 13. For cresyl violet emission spectra, a 2nd-order polynomial was used.

Integration of emission peaks for use in quantum yield calculations was calculated using

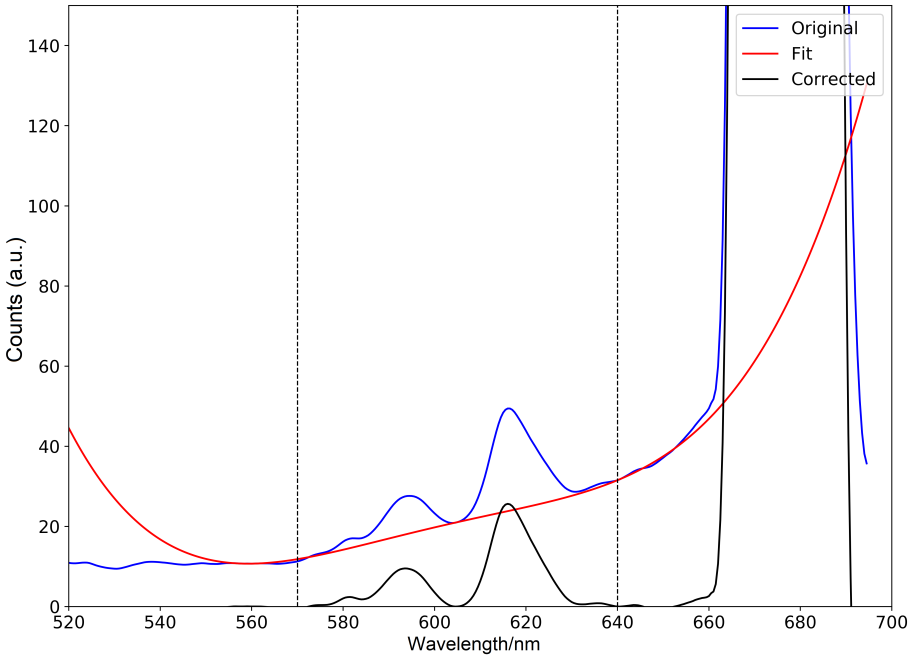

Figure 13. Example of the background correction of Eu^{3+}-center luminescence using the numpy.polyfit function. The area between the vertical dotted lines represent the area of interest to be integrated for use in quantum yield calculations.

the trapz function of the numpy module.

All FTIR spectra were pre-processed using a min-max normalization method:

$$x' = \frac{x - min(x)}{max(x) - min(x)} \tag{3}$$

CHAPTER THREE: RESULTS & DISCUSSION

TTA-Coated Europium-Doped Calcium Fluoride Nanoparticles

Synthesis

In adapting the Lin Ma *et al.* synthesis from a microwave oven to a microwave reactor, there were a few issues to overcome: the wattage, the chemical used to adjust the pH (NaOH), a transparent product solution, and the fluoride ion source, $NaBF_4$.[16] The reported synthesis conditions for their microparticles were 40 minutes in a 650 W, 2.45 GHz oven at 80 % power. This poses an issue due to conventional microwave ovens typically using 30 second power cycles. 50 % power would mean that the microwave is running at 650 W for 15 seconds and 0 W for 15 seconds, cycling. Whereas with a 300 W laboratory microwave reactor, 50 % power will cause the instrument to output 150 W.

The original publication reported adjusting the pH of the solution to 6.0 using 10 % nitric acid solution, but the pH of the reactant solution before adjustment was about 3.0. In our work, 4.0 M NaOH solution was used to raise the pH instead. Different pH levels were investigated to discover their effects on the synthesis, but a pH of 6.0 was found to yield the best results. Syntheses using pH values above 6 were inconsistent, while values below 6 yielded larger-sized particles and greater size dispersions.

Originally, an older sample of 95 % pure $NaBF_4$ was used in the synthesis. Part of the impurities were insoluble in water and yielded a slightly cloudy solution, but nonetheless worked well. A new sample of 98% pure $NaBF_4$ was ordered, and it's impurities were soluble in water. However, using this sample in our synthesis yielded much larger sized nanoparticles as confirmed by DLS measurements relative to the 50-100 nm product using the old bottle of $NaBF_4$. Figure 14 shows the size distribution of the product using this sample of $NaBF_4$. Simple changes in the method to make smaller nanoparticles using this new sample were largely unsuccessful. It is hypothesized that the insoluble impurities from the first $NaBF_4$ sample were influencing crystal

growth by acting as a nucleation site for new crystals.

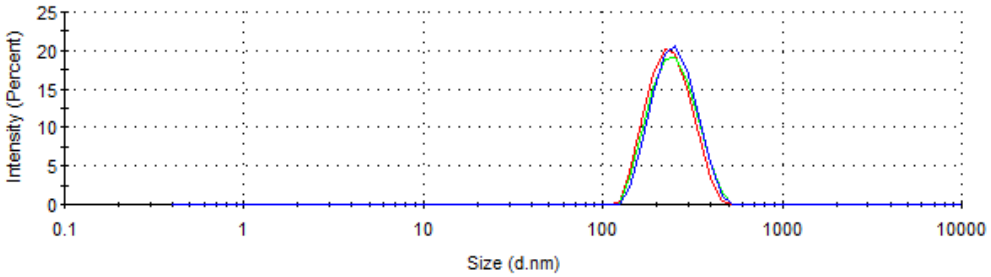

Figure 14. Size distribution of nanoparticle product synthesized using the new bottle of $NaBF_4$.

A decision was made to first try a method on the instrument that uses constant power throughout the entirety of the runtime. An arbitrary value of 100 W was selected as a baseline, and it yielded results similar to that reported by Lin Ma *et al.* when refluxed for the original 40 minutes as seen in Figure 15. The average size of the nanoparticles was 1019.2 nm, which is in the 1000-1100 nm range reported by Lin Ma *et al.*[16]

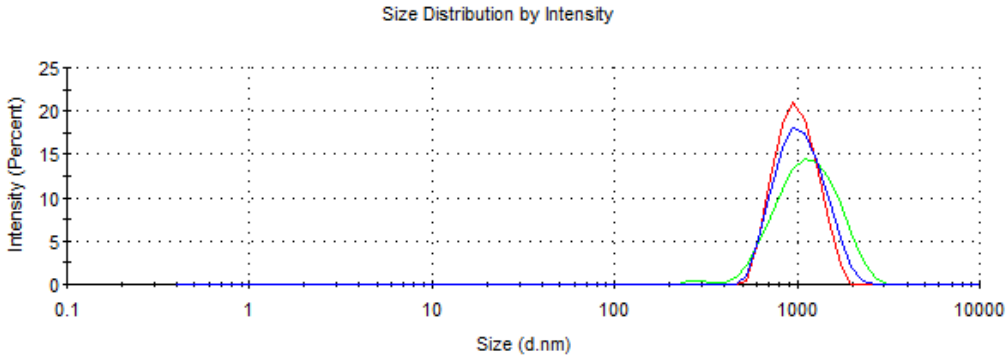

Figure 15. The size dispersion of the first successful synthesis of Lanthanide-dope CaF_2 nanoparticles.

The attempts to reduce the average size of nanoparticle product by increasing the overall

concentrations was successful. The original overall concentration for metal chlorides (calcium chloride and europium chloride) was 0.020 M. The concentration was stepped up in 100 % increments. These results are shown in Table 2. An overall metal chloride concentration of 0.065 M seemed to be approaching a limit in terms of decreasing the average particle size. Increases in concentrations beyond this point either yielded a small amount of progress or diminishing returns. For producing nanoparticle product that is smaller than 50-60 nm, simply decreasing the synthesis time should be sufficient.

Table 2. Relationship of overall metal chloride concentration to average nanoparticle size.

Metal Chloride Conc./M	**Average Size /nm**
0.020	1019.2
0.040	457.6
0.060	200.2
0.065	66.1

Purification of the nanoparticle product proved challenging, as the resultant solution after reaction in the microwave was clear and colorless when particle size was less than about 120 nm. Average particle sizes larger than 120 nm yielded progressively white cloudy solutions. The only confirmation that product existed below this size was found through DLS measurements. Short centrifuge times (10-15 minutes) at moderate speeds (3000-4000 rpm) were insufficient in separating dispersed nanoparticles from the reactant solution, but it was found that extended centrifuge times (2-4 hours) at relatively higher speeds (5000-6000 rpm) were sufficient in creating a pellet of the nanoparticle product at the bottom of the centrifuge tubes. Due to the pellet itself appearing transparent as shown in Figure 16, a UV lamp set to 325 nm was used to affirm that the pellet was europium-doped product. Figure 17 shows this pellet under excitation by UV radiation. The supernatant solution did not exhibit luminescence. Figure 18 shows a range of purified

and dried nanoparticles illuminated by a UV lamp, from 2.5-35% Eu^{3+} theoretically doped CaF_2.

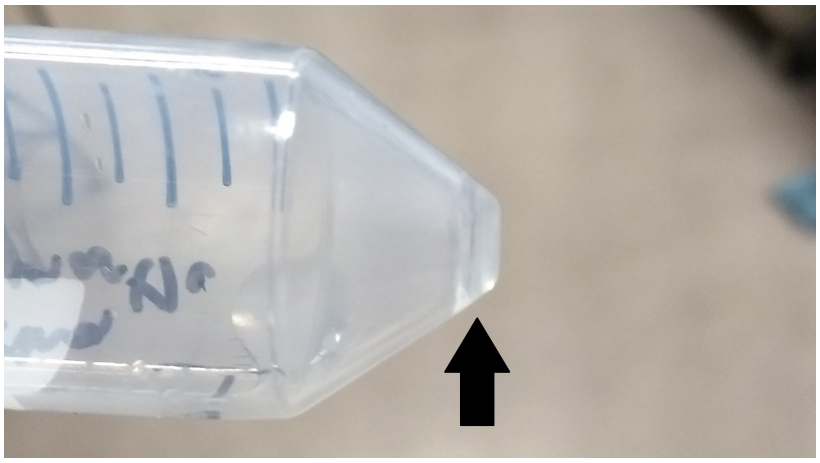

Figure 16. Transparent product pellet in reaction solution after being centrifuged at 6000 rpm for 3 hours.

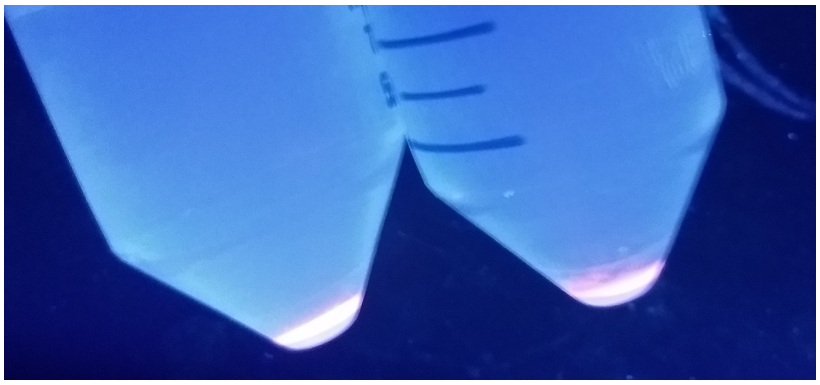

Figure 17. Transparent product pellet in centrifuge tube after being centrifuged at 6000 rpm for 3 hours, under illumination by UV lamp set to 325 nm.

For the synthesis as described, an average yield of 118.7 +/- 42.8 mg (N=12) is more than fair especially considering how high-quality the product is.

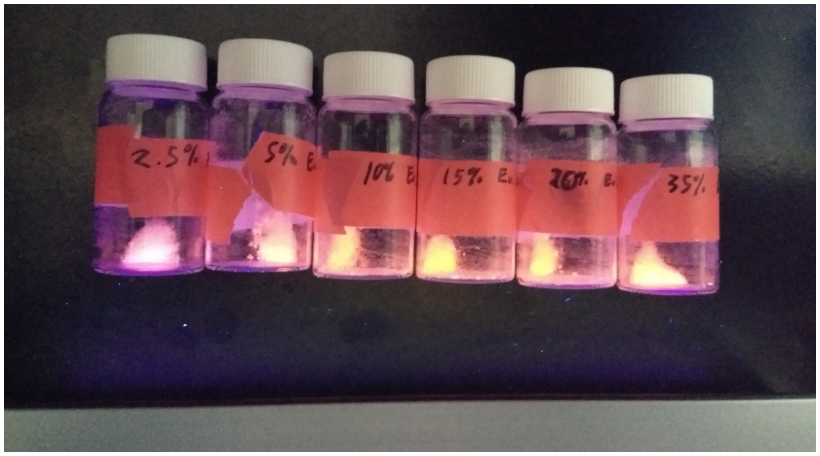

Figure 18. From left to right: 2.5, 5, 10, 15, 20, and 35% theoretically Eu-doped CaF_2 dry nanoparticle product under illumination from a UV-lamp set to 325 nm.

Nanoparticle Morphology

Dynamic light scattering (DLS) was used as a qualitative measurement of the size dispersion of the nanoparticles, while transmission electron microscopy (TEM) was used as a quantitative measurement of size dispersion and shape of product. The Scherrer equation was used in conjunction with XRD spectra to estimate the crystallite size.

Using the method parameters in the previous section, the nanoparticles typically have a size distribution as described by the DLS measurement in Figure 19. DLS measurements of TTA-coated samples using neat methanol as the dispersant yielded peaks representing the correct size range for the nanoparticle product and other peaks representing possible aggregations. TTA-coated samples that were measured in 1:1 methanol:water mixture yielded data that was similar to the uncoated samples, but still inconsistent. The presence of water likely quenched the luminescent efficiency of the samples enough for a rough estimate of the size dispersion of product. In pure water, the dispersibility of TTA-coated nanoparticles may be very low due to the hydrophobic nature of TTA.

TEM images showed 35 % Eu^{3+}-doped CaF_2 nanoparticles to have a flower-like shape, shown in Figure 20. Also shown is the high monodispersion of nanoparticles, and lattice lines,

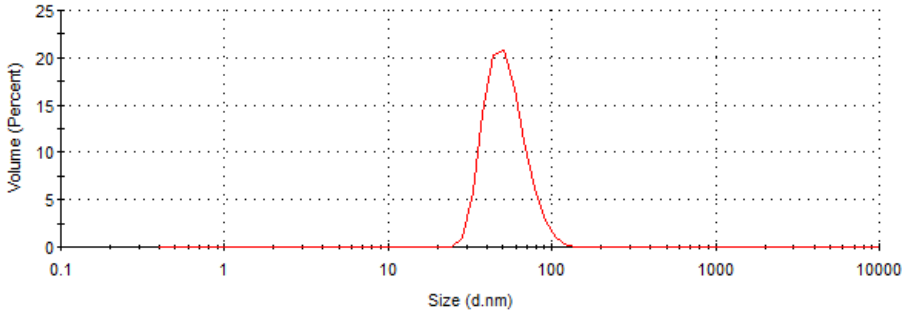

Figure 19. Dynamic Light Scattering data representing the size distribution of a typical Eu^{3+}-doped CaF_2 nanoparticle synthesis with an overall metal chloride concentration of 0.065 M.

which are evidence of the high crystallinity of the nanoparticles. This rougher flower-like structure differs from the microspheres found by the original publication.[16] Each flower-like structure appears to be composed of multiple spherical structures, which are likely individual crystallites. For 35 % Eu^{3+}-doped CaF_2, the crystallite size was about 10.7 nm as estimated by the Scherrer equation. The size of the spherical structures roughly correlates to the estimated crystallite size.

Figure 21 compares four different samples. Image a and b compare TTA-coated nanoparticle product to untreated EDTA-coated nanoparticle product, respectively. No difference is found aside from the greater aggregation of TTA-coated product, which is expected due to the non-polar properties of TTA, evident of the tendency for these molecules to be attracted to one another. Some difference in shape is seen between pure CaF_2 nanoparticle product and 35 % Eu^{3+}-doped CaF_2 nanoparticle product. Pure CaF_2 has less of the flower-like shape and is more spherical. This suggests that the presence of Eu^{3+} in the synthesis is influencing the flower-like shape. Also shown in Figure 21 are Eu^{3+}-doped CaF_2 nanoparticle samples whose syntheses used different heating sources. One used microwave irradiation, while the other used a heating mantle. The flower-like shape is evident in both of these samples, showing that microwave irradiation has little to no effect on the morphology in comparison to heating with convection. A range of sam-

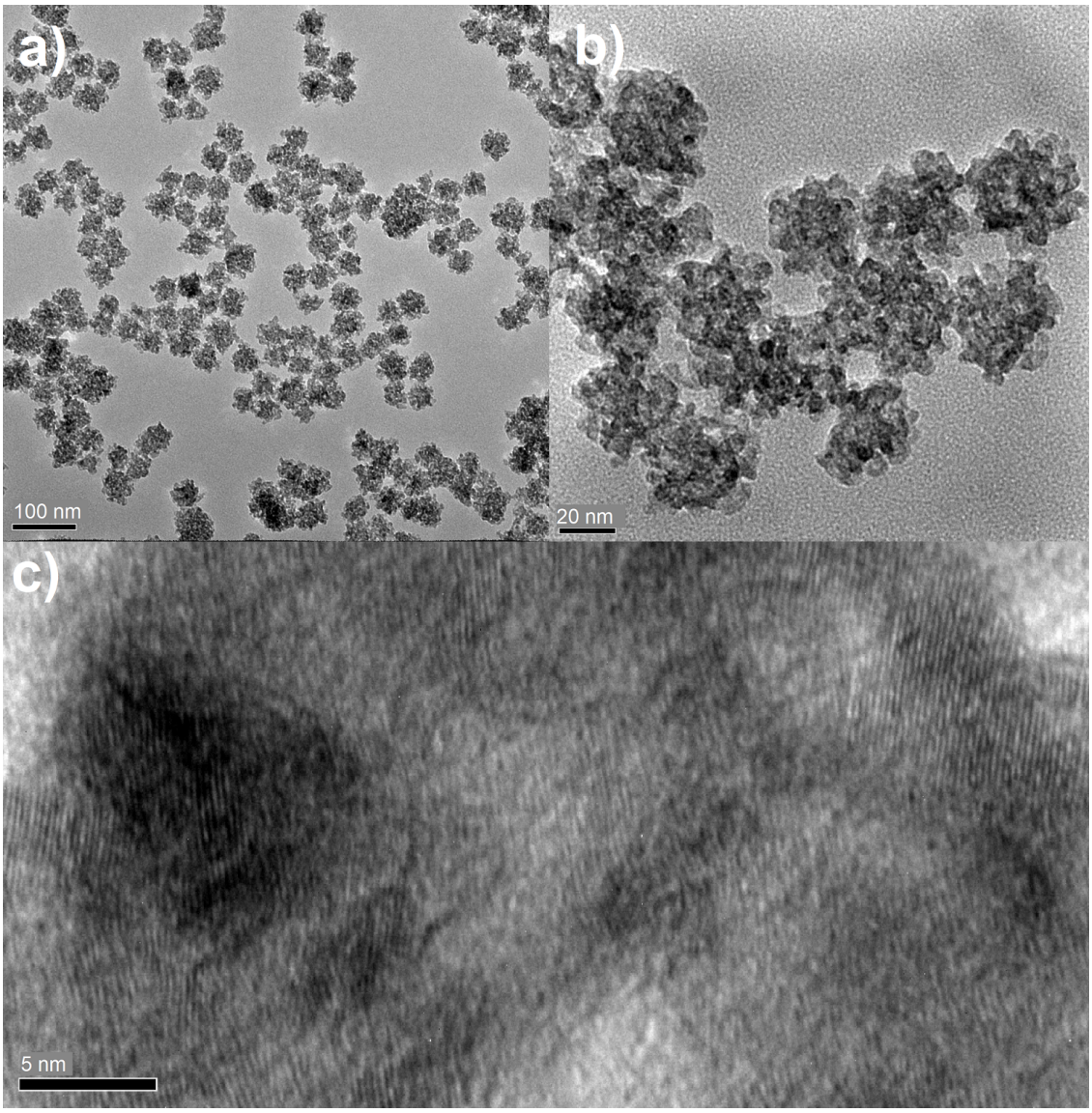

Figure 20. TEM images of 35 % Eu^{3+}-doped CaF_2 nanoparticles. a) low magnitude image showing the monodispsersity, b) medium magnitude image showing the flower-like structure, c) high magnitude image showing the crystalline lattice lines.

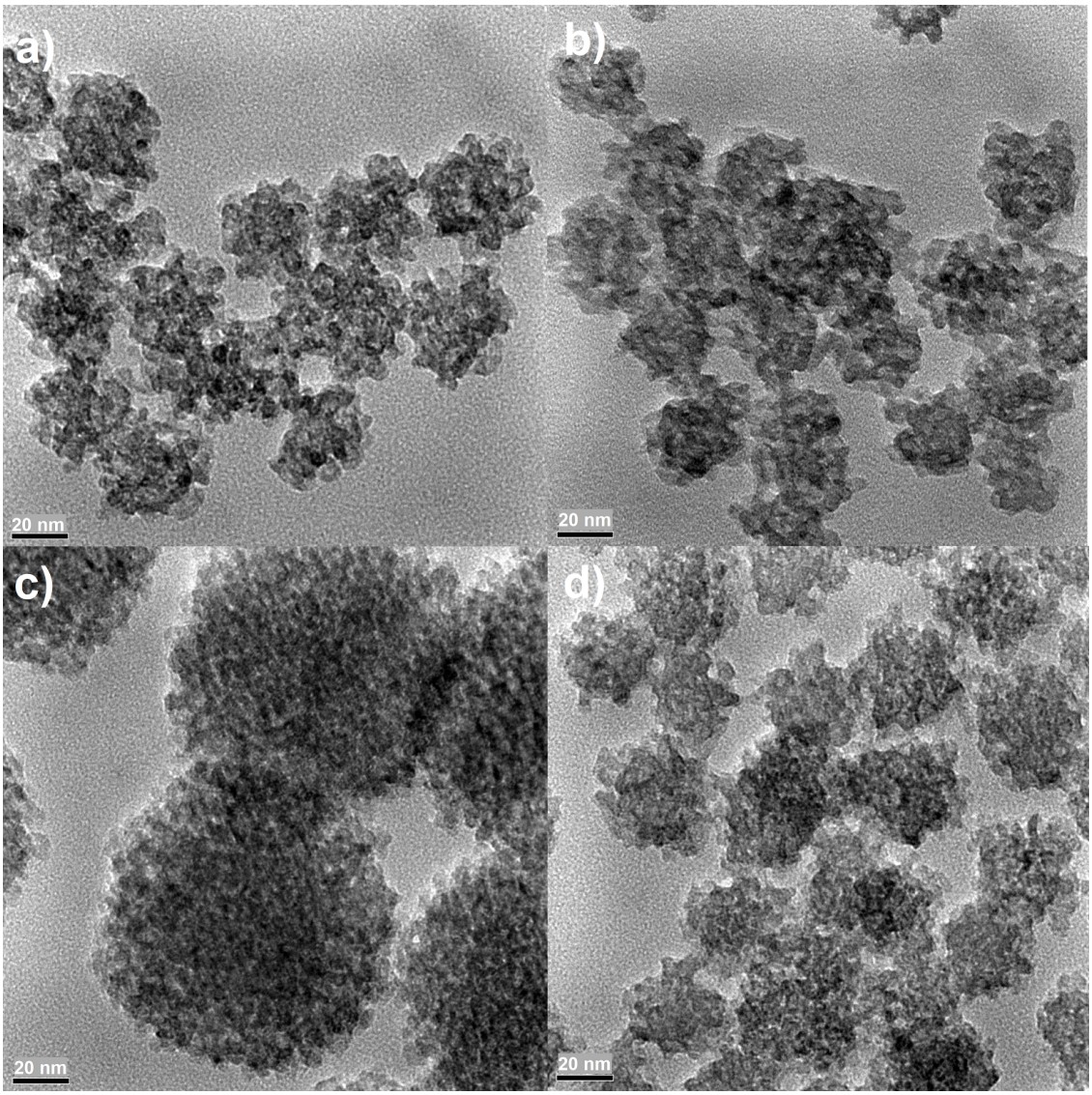

Figure 21. TEM images of Eu^{3+}-doped and pure CaF_2 nanoparticles. a) 35 % Eu^{3+}-doped CaF_2, b) TTA-coated 35 % Eu^{3+} CaF_2, c) pure CaF_2, d) 20 % Eu^{3+} CaF_2 using a traditional heating source instead of microwave irradtiation.

ples with various % doping of europium are shown in Figure 22. This figure shows the change in structure as the amount of europium doped into the CaF_2 crystal matrix increases.

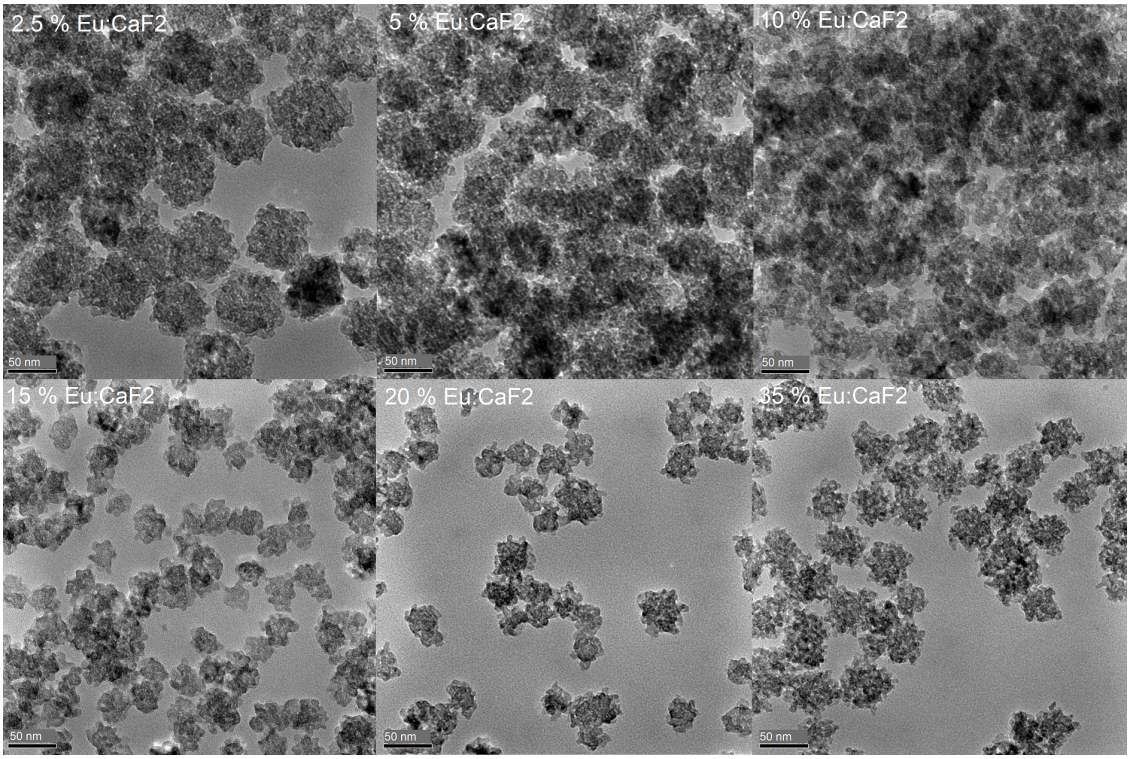

Figure 22. TEM images of various % dopings of Eu^{3+}:CaF_2 nanoparticle product.

Scanning Electron Micrographs show similar results. The flower-like structure of the nanoparticle product is shown again in Figure 23, with some of the 3-D structure also shown when zoomed in.

Using a low magnification TEM image of 35 %-doped Eu^{3+} CaF_2, 100 particles were measured using the reference ruler. The average size found using this method was 43.6 +/- 6.7 nm. The size dispersion of this data is shown in Figure 24.

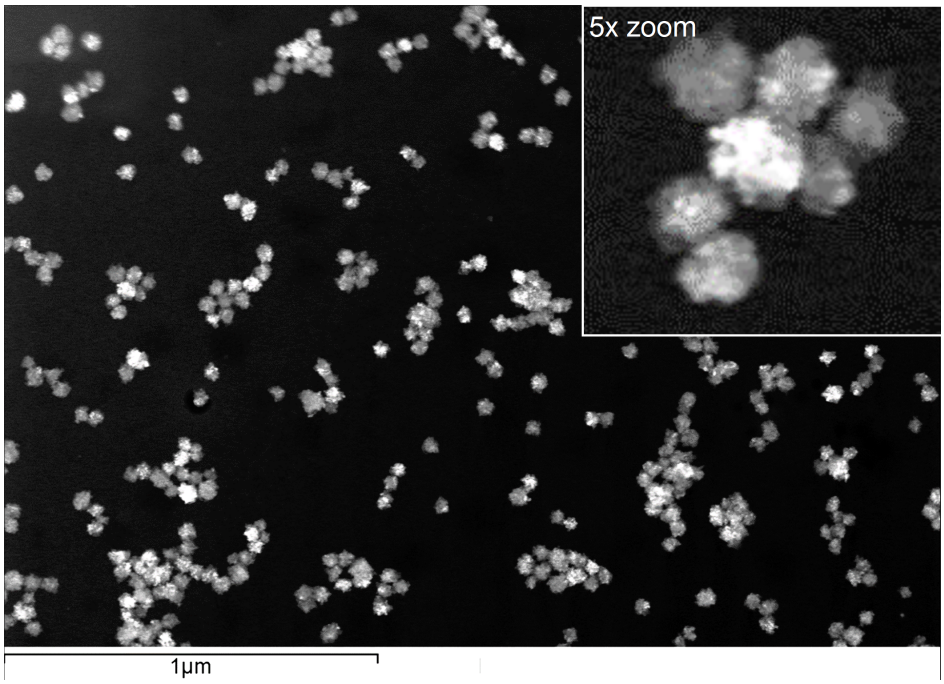

Figure 23. SEM image of 35 % Eu^{3+}-doped CaF_2 nanoparticles.

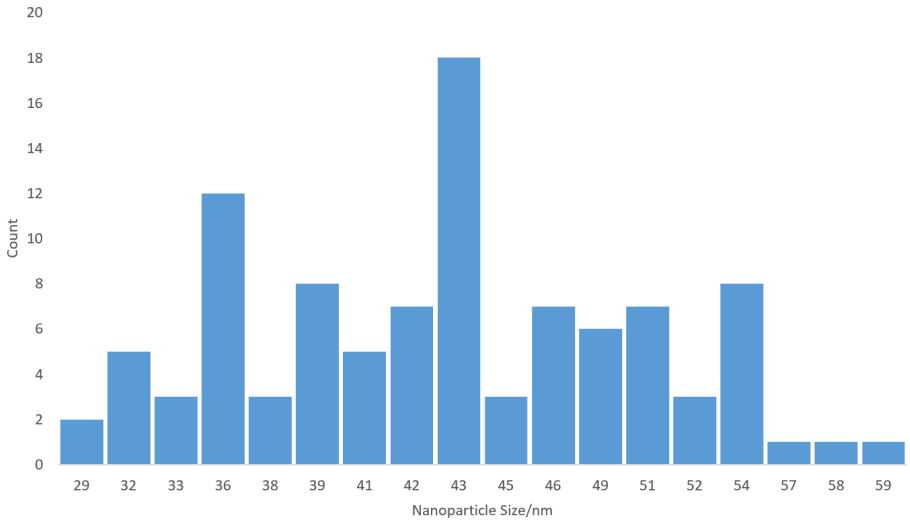

Figure 24. Plot representing the size distribution of Eu^{3+}-doped CaF_2 nanoparticle product. (N=100)

Energy-dispersive X-ray Spectroscopy

The elemental composition of Eu^{3+}-doped CaF_2 nanoparticle product was studied using EDX. This data is shown in Figure 25. The large peak for calcium is likely combined with the signal from carbon.

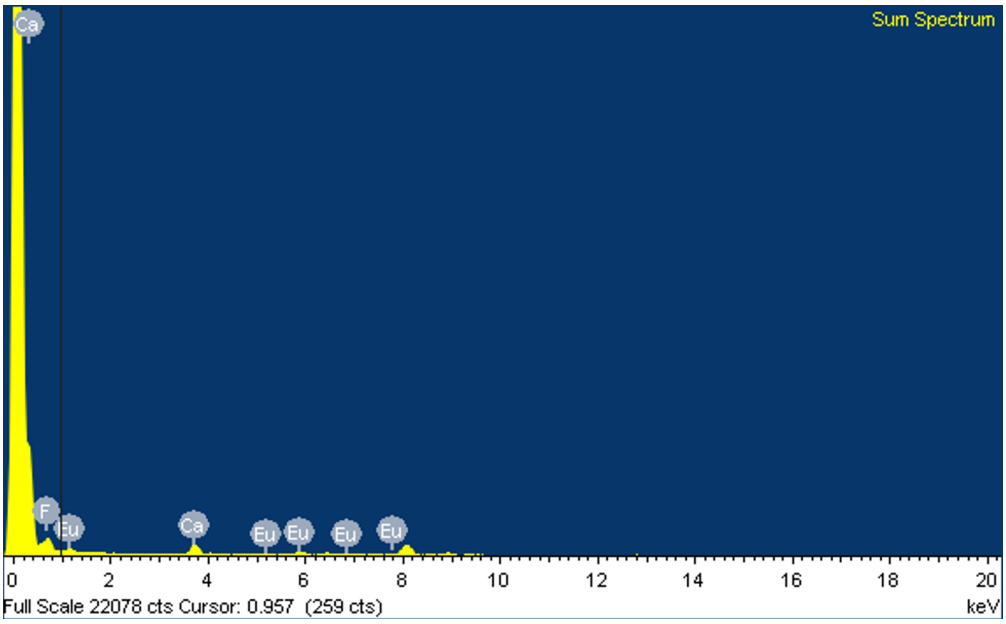

Figure 25. EDX graph of 35 % Eu^{3+}-doped CaF_2 nanoparticles.

Crystalline Purity

Powder X-ray diffraction was used to determine the changes in crystalline purity as the theoretical % doping amounts of Eu^{3+} ions into the CaF_2 crystal matrix increased.

Figure 26 shows a typical XRD spectrum of Eu^{3+}-doped CaF_2 nanoparticles with labeled facets.[29,30] Other peaks with relatively very small peak intensity not attributed to CaF_2 may be from the presence of a mixture of hydroxylapatite ($Ca_5(PO_4)_3(OH)$) and fluorapatite ($Ca_5(PO_4)_3F$) impurities.[29,31] The hydroxide impurities were expected since the synthesis is aqueous. The phosphate impurities are likely from the calcium chloride reagents.

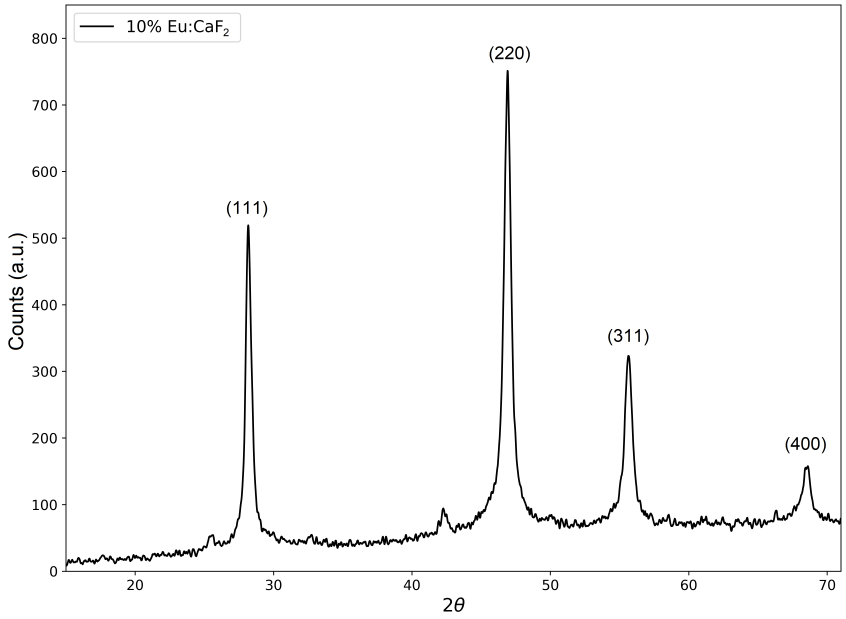

Figure 26. P-XRD spectrum of prepared 10% Eu^{3+}-doped CaF_2 nanoparticles.

Figure 27 shows the spectra of reagent CaF_2 versus synthesized CaF_2 nanoparticles. Differences in bandwidth are due to the difference in particle size, and the slight shift in peaks can be attributed to differences in instrument response as these two samples were measured multiple months apart. Aside from those differences, these spectra are in good agreement providing proof that CaF_2 is indeed the product.

Due to the success of synthesizing nanoparticles using the same method conditions but using a traditional heating source, there was interest in looking for differences in XRD patterns when compared to the microwave-based method. In Figure 28, no difference is evident in the spectra. The aforementioned slight peak shift can be attributed to the difference in instrument response when measurements are taken multiple months apart.

Aside from the minor impurities, the main point of interest that was found in spectra was the downwards shift of peaks as Eu^{3+} concentrations increased in the CaF_2 matrix. Shown in Fig-

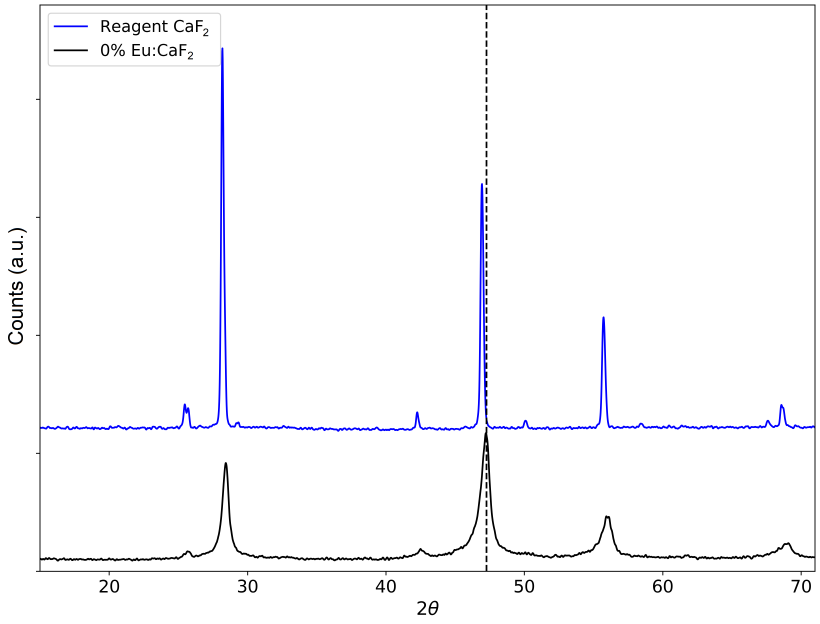

Figure 27. P-XRD spectra comparing reagent CaF_2 against synthesized CaF_2 nanoparticles.

ure 29 with multiple vertical dotted lines for reference, there was a difference of -0.396 2θ between the 0% and 35% Eu^{3+}-doped samples for the peak centered about 28 2θ and a difference of -0.528 for the peak centered about 47 2θ. The strain that the increased introduction of Eu^{3+} has on the CaF_2 crystal structure is likely the cause of these peak shifts.

The Scherrer equation was used with P-XRD data to estimate the crystallite size of the nanoparticle product.

In all cases, the crystallite size was smaller than the average nanoparticle size as determined by DLS (50-60 nm for these samples). Interestingly, the crystallite size increased from 0% to 5% Eu^{3+}, then decreased from 5% to 35%.

Determination of Actual Concentrations of Doped Europium Ions

The ratio of signal of Eu^{3+} to Ca^{2+} peaks in relation to known calibration standards was used to determine the actual concentrations of Eu^{3+} ions doped into the CaF_2 crystal matrix using

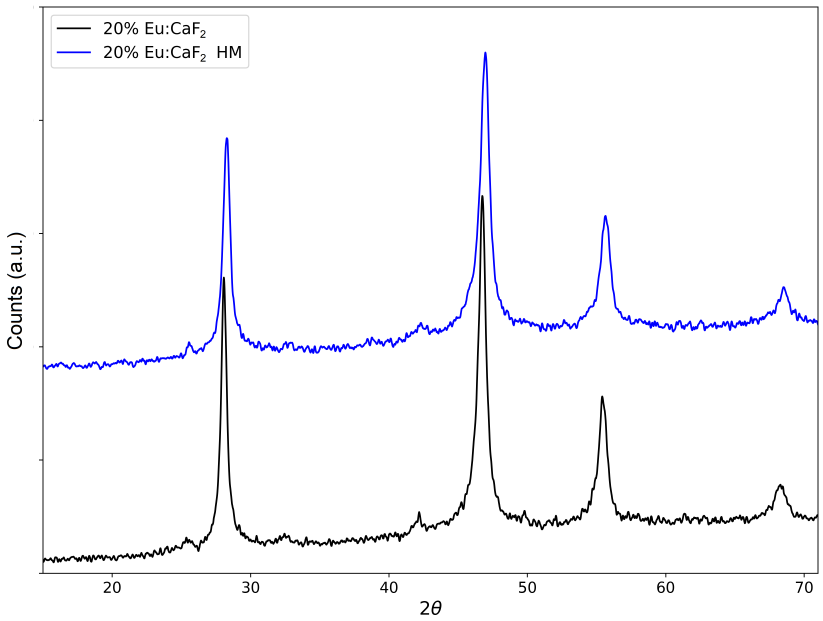

Figure 28. P-XRD spectra comparing two 20% Eu:CaF_2 samples, one prepared in the microwave and the other using a heating mantle (HM).

Table 3. Estimated crystallite sizes using the Scherrer equation.

% Eu^{3+}:CaF_2	**Average Crystallite Size /nm**
0	12.83
2.5	21.96
5	26.40
10	16.45
15	12.78
20	11.56
20HM	9.91
35	10.71

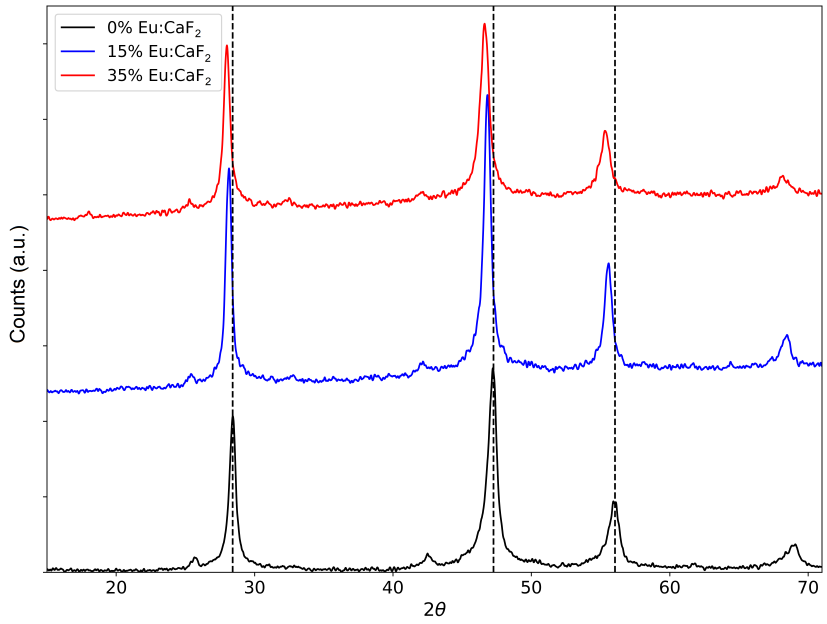

Figure 29. P-XRD spectra showing the downwards shift in peak position as Eu^{3+} concentrations increase in the CaF_2 matrix.

the microwave-assisted method described. Due to NaOH being used to adjust pH during synthesis, the concentration of Na^+ ions was analyzed as well.

Table 4. Actual concentrations (% w/w) of Europium(III) ions in doped CaF_2 nanoparticles. HM is Heating Mantle, representing a traditional heating method in contrast to the microwave-assisted method.

Theoretical/%	**Actual/%**	**STD/% (N=3)**	**% Diff.**
2.5	9.8	1.6	118.9
5.0	15.8	1.2	103.9
10.0	23.1	0.1	79.2
15.0	28.0	0.2	60.3
20.0	32.2	1.2	46.7
20.0 HM	26.6	0.8	28.4
35.0	38.0	0.5	8.3

No signal for sodium ions was found in any sample, so it's data was not included.

Using the method of least squares, lines of best fit were calculated to find the actual concentrations of samples as shown in Table 4. Actual europium concentrations (in %) in doped CaF_2 nanoparticle product were considerably higher than theoretical, though this difference decreased as the % doping increased. Firstly, although EDTA is known to bind more strongly to trivalent (Eu^{3+}) ions than divalent (Ca^{2+}), how the microwave energy interacts with Eu[EDTA] complexes may be vastly different than with Ca[EDTA]. If the microwave energy interacts strongly with Eu[EDTA] complexes relative to Ca[EDTA] or it's respective intermediates, this may cause the Eu^{3+} ions to dissociate from EDTA faster and yield nanoparticles with higher % Eu^{3+} concentrations. Second, there may have been errors regarding the calculation and usage of the metal chloride starting materials. As the metal chlorides used were hydrated reagents, an older reagent bottle that was not flushed with nitrogen before storage may have absorbed water from the air. In hindsight, titrations to ascertain the hydration of the metal chloride reagents would have elimi-

nated this as a potential issue.

Another result from this data is the difference in doping between the microwave-assisted method and the traditionally heated method using a heating mantle. For CaF_2 samples that were theoretically 20% Eu^{3+}, the microwave-assisted method had an average (N=3) Eu^{3+} concentration of 32.2% while the heating mantle method yielded an average (N=3) of 26.6 %. Due to the microwave method having a higher % yield, this may further support the theory of the microwave energy directly influencing the dissociation rate of Eu^{3+} from Eu[EDTA] complexes.

Fourier-Transform Infrared Spectroscopy Studies

Fourier-Transform Infrared Spectroscopy was used to identify the surfactants of nanoparticles from the described method and to quantify the TTA coating of nanoparticle product. $Eu[TTA]_3[H_2O]_2$ complexes and pure reagents of EDTA and TTA were also measured to aid in identification. All spectra were normalized to a range of 0-1 using a min-max method. Spectra were also truncated to 2000-650 cm^{-1}. Due to the relatively small amount of organic material bound to the surface of nanoparticles, low amounts of signal were expected for IR spectra of samples.

Since the microwave-assisted Eu^{3+}-doped CaF_2 nanoparticle synthesis uses an excess of EDTA as a surfactant and EDTA complexed with metal ions, it was expected that the resultant product was going to be coated with EDTA. The sample spectrum in Figure 30 shows the carbonyl band at 1600 cm^{-1}, and relatively diminished bands in the fingerprint region (less than 1400 cm^{-1}) possibly due to the influence of the EDTA being bound to either Ca^{2+} or Eu^{3+} on the surface of the particles. Some of the four peaks between 1400-1300 cm^{-1} in pure reagent EDTA may be attributed to the various C-N bonds in EDTA. All of these peaks underwent reduction in intensity upon EDTA being bound to the surface of product.

There are a few key differences between pure reagent TTA and TTA bound in Eu^{3+}-based complexes, shown in Figure 24. Most notable is the shift of the carbonyl from 1650 to 1610 cm^{-1}. This type of shift was not observed with EDTA in Figure 30. It is hypothesized that the energies of the TTA carbonyl bonds change upon being complexed with Eu^{3+}.

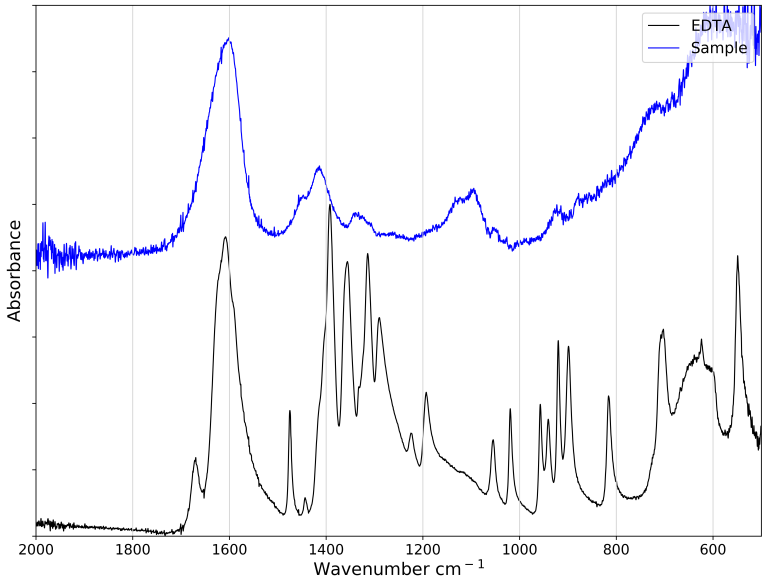

Figure 30. FTIR spectra comparing pure reagent EDTA against EDTA-coated CaF_2 nanoparticles.

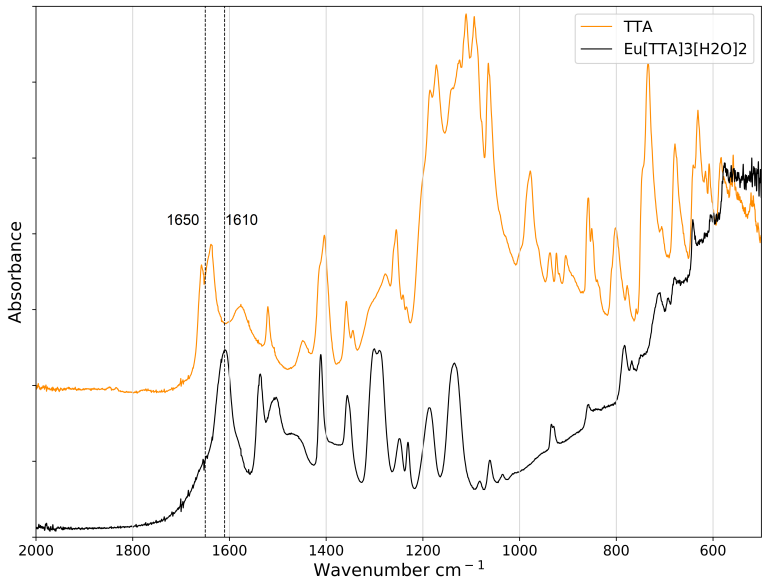

Figure 31. FTIR spectra comparing pure reagent TTA with $Eu[TTA]_3[H_2O]_2$ complexes.

The key point of FTIR studies for this project is quantifying the presence of TTA on the surface of the nanoparticle product. Figure 32 shows the difference in spectra after the TTA coating procedure. The most notable differences are an increase in peaks throughout the fingerprint region, a likely duet of peaks between 1550-1500 cm^{-1}, and a significant peak at 1410 cm^{-1}. All of these are represented in the TTA-coated CaF_2 spectra, shown in Figure 33, which compares the product to Eu[TTA] complexes and EDTA.

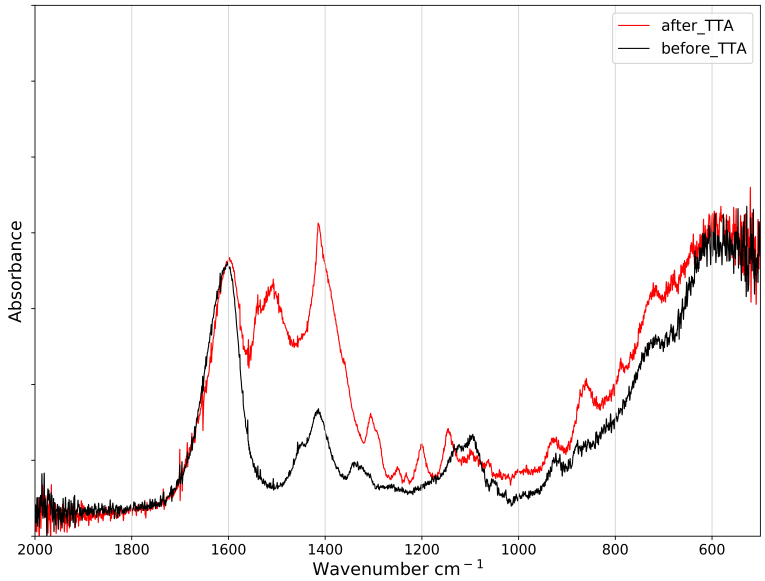

Figure 32. FTIR spectra comparing a CaF_2 nanoparticle product before and after the TTA coating procedure.

UV-Vis Absorption Studies

To help affirm the presence of TTA ligands on the surface of the nanoparticle product, various UV-Vis spectra were taken. EDTA, TTA, and reagent CaF_2 were analyzed as shown in Figure 34. EDTA showed no absorbance until the far-UV, TTA had a single irregular band at 240-400

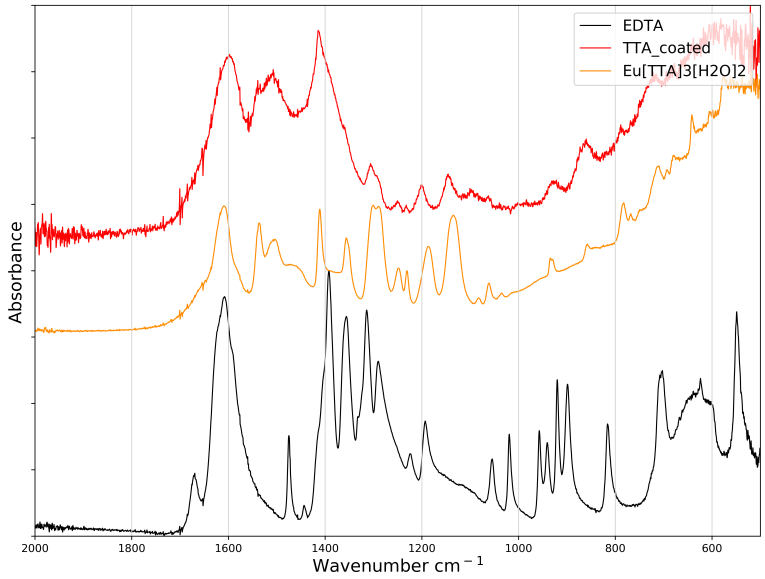

Figure 33. FTIR spectra comparing TTA-coated CaF_2 nanoparticle product, $Eu[TTA]_3[H_2O]_2$ complexes, and pure reagent EDTA.

nm, while CaF_2 held steady absorbance throughout the entire spectrum that was proportional to the concentration. A composite of EDTA and reagent CaF_2 was expected for the initial nanoparticle product and is shown in Figure 35. For these, changing the amount of Eu^{3+} doped into the CaF_2 product did not change the spectra, and so only one is shown.

Similar UV-Vis absorption spectra that were found for $Eu[TTA]_3$ complexes were expected in TTA-coated Eu^{3+}-doped CaF_2 nanoparticle product.[15] The primary peak has a λ_{max} of 340-341 nm.

In Figure 36, a UV-Vis absorption spectrum nearly identical to the one found in literature is shown. The λ_{max} that was expected at 340-341 nm is marked by a vertical dashed line. A notable difference in the absorption of free TTA and TTA chelated to Eu^{3+} was seen when compared to Figure 34. This is likely due to a change in energies within the molecule upon being coordinated to a metal ion.

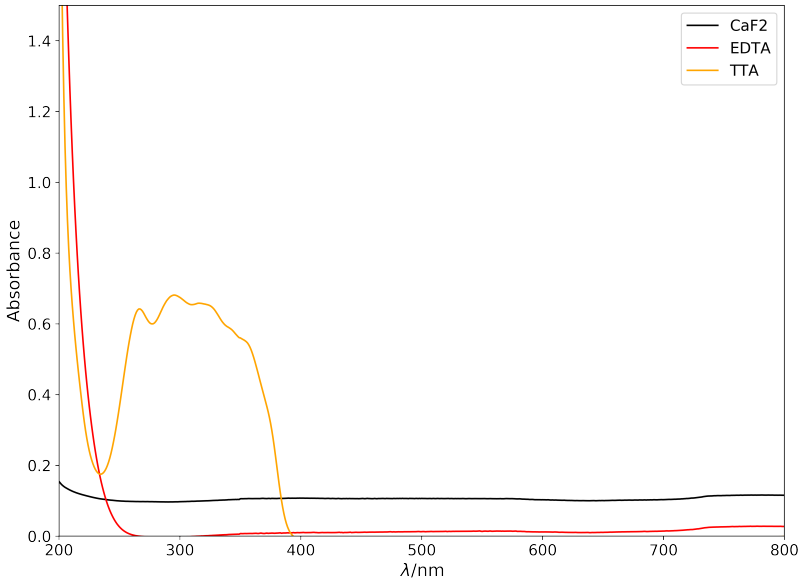

Figure 34. Composite UV-Vis absorption spectra of EDTA, TTA, and reagent CaF_2.

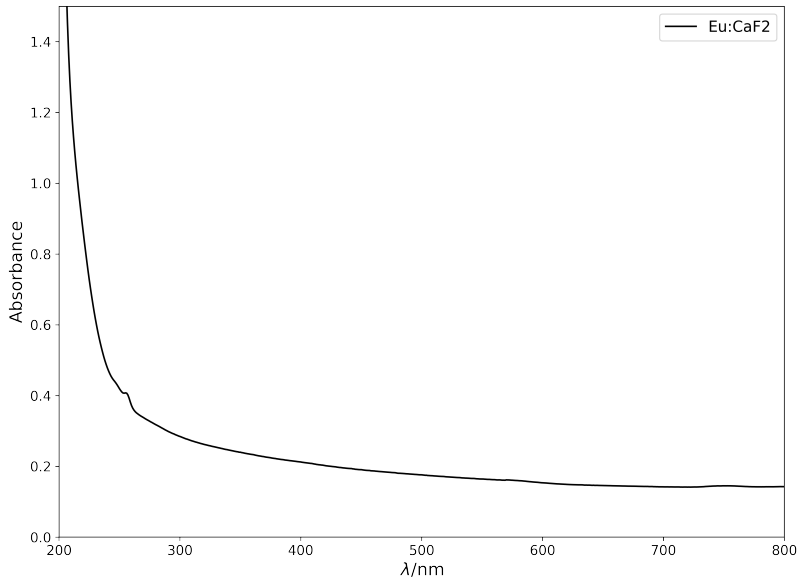

Figure 35. UV-Vis absorption spectrum of initial Eu^{3+}-doped CaF_2 nanoparticle product before being coated with TTA.

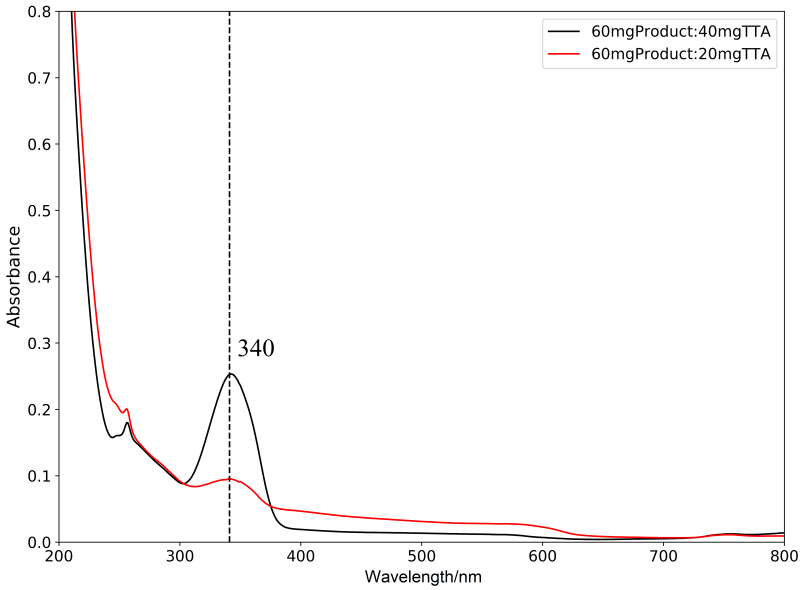

Figure 36. UV-Vis absorption spectrum of two samples of TTA-coated nanoparticle product, showing the max absorption peak indicitive of TTA ligands.

Luminescent Studies

Fluorometry was used to quantify the emission and excitation of Eu^{3+}-doped CaF_2 nanoparticle product. A qualitative emission spectra of nanoparticle product is shown in Figure 37.

In excitation studies, the emission wavelength was held constant at 617 nm while the excitation wavelength was scanned. It is essential to select the excitation wavelength that yields the greatest emission in order to maximize the quantum yield. As shown in Figure 38, the expected excitation wavelength to yield maximum emission was seen at 340 nm.

Emission studies were initially complicated by 2nd-order diffraction. Due to excitation at 340 nm, a peak at twice that wavelength at 680 nm was observed. Even though analyte solutions were clear, a significant amount of light scattering from the nanoparticle product was evident. In most cases for samples containing relatively low amounts of Eu^{3+}, the amount of signal from the 2nd-order diffraction peak at 680 nm was enough to significantly diminsh the signal-to-noise ra-

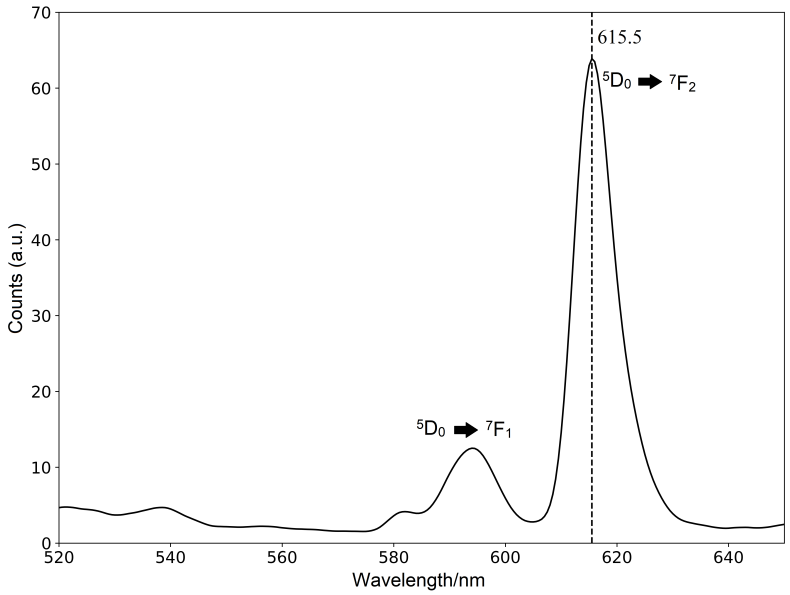

Figure 37. Qualitative emission spectrum of TTA-coated Eu^{3+}-doped CaF_2 nanoparticles, excited at 340 nm.

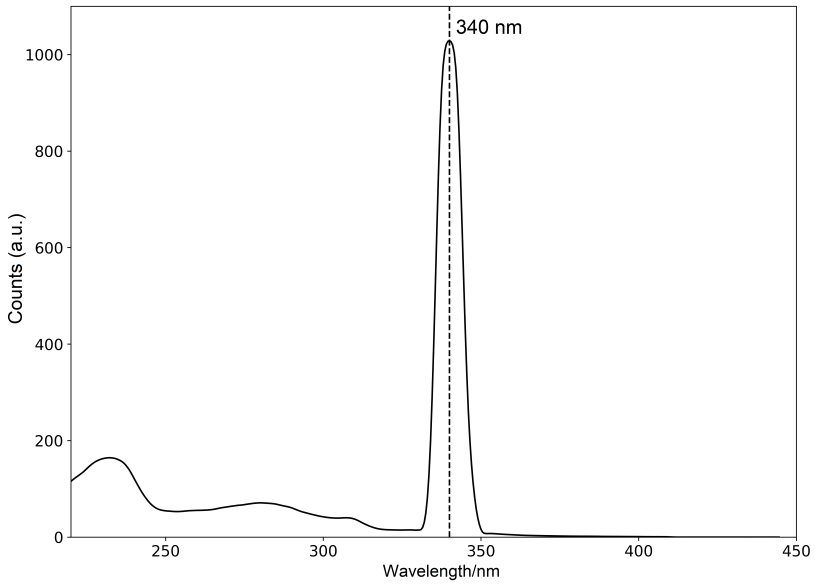

Figure 38. Qualitative excitation spectra of TTA-coated Eu^{3+}-doped CaF_2 nanoparticles.

tio as shown in Figure 39. Counterintuitively, this was solved by increasing the concentration of the analyte until absorbance at 340 nm was 0.4-0.6. These spectra were then fitted with a polynomial function for background subtraction as shown eariler in the Chemometrics section of the Experimental chapter.

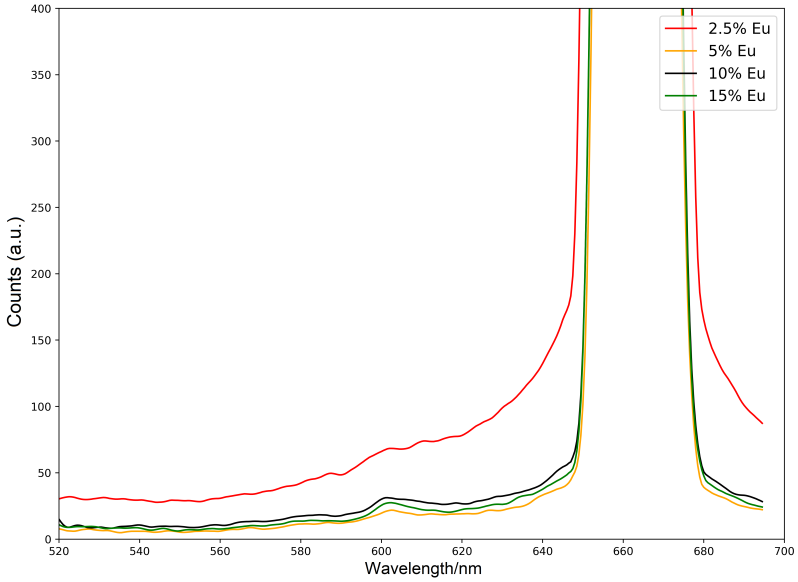

Figure 39. Emission spectra of various TTA-coated nanoparticle samples showing low signal:noise.

Quantum Yield Studies

Table 5 shows the results of the quantum yield measurements. All samples were coated using the 40 mg product:50 mg TTA ratio as described in the experimental except for 15A which used a lower concentration of 40 mg nanoparticles:25 mg TTA. The lower concentration sample yielded a lower percent quantum yield, 0.31 +/- 0.03 % versus 1.53 +/- 0.41 % for the higher concentration. This shows that a higher concentration of TTA yields a better result, at least in the

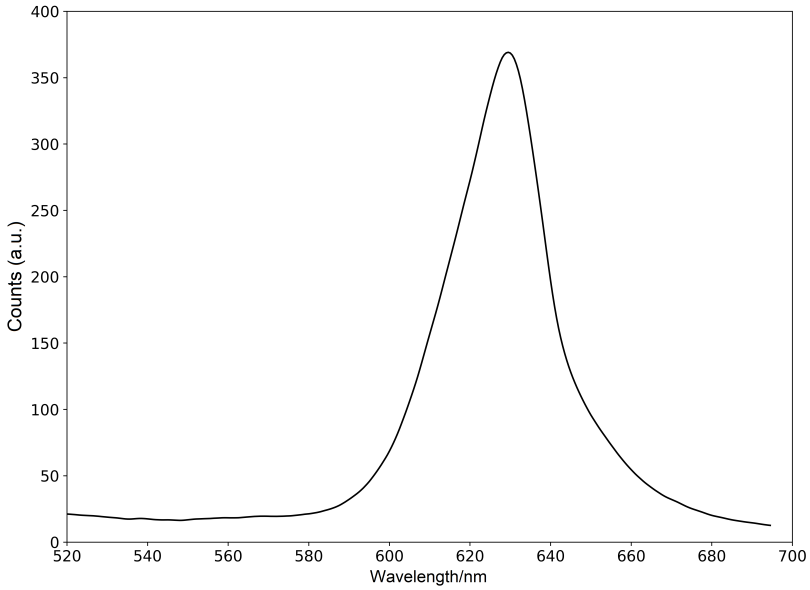

Figure 40. Qualitative emission spectra of cresyl violet acetate, excited at 317 nm.

case of the 15% Eu:CaF_2

These low quantum yield values may be due to both their transparency and light scattering abilites. CaF_2 is well known to be transparent from the UV through the IR range. This transparency may be preventing the absorption of light by both the TTA molecules on the surface and europium ions contained within these nanoparticles. Nanoparticles are also well-known for their light scattering abilities, and this may be further reducing their quantum yield by a similar manner.

Table 5. Quantum yields of various TTA-coated Eu^{3+}-doped CaF_2 nanoparticle samples.

% Eu:CaF_2	**Quantum Yield/%**	**STD (N=9)/%**
2.5	0.25	0.08
5	0.36	0.05
10	0.78	0.22
15A	0.31	0.03
15	1.53	0.41
20	1.10	0.37
35	1.41	0.37

CHAPTER FOUR: CONCLUSIONS

The optimization of the synthesis was successful, though a lower limit (20-30 nm) of the average particle size was found while increasing the overall metal chloride concentrations. Shortening the synthesis time should be successful in reaching smaller average particle sizes. S/TEM imagery showed that the Eu^{3+}-doped CaF_2 nanoparticle product had a flower-like morphology. It is hypothesized that the presence of Eu^{3+} and EDTA influenced the growth and therefore the structure of the nanoparticles, whereas the heating source did not (microwave versus traditional heating). As described, the method produces nanoparticles with an average size of 43.6 +/- 6.7 nm (N=100) as measured using TEM images. TTA (thenoyltrifluoroacetone) coatings of nanoparticles were successful, particularly to the naked eye when excited by a UV lamp. This was confirmed further through FT-IR and UV-Vis absorption measurements. While at first complicated by the 2^{nd}-order diffraction of the fluorometer, luminescent quantum yield measurements were successful through the use of chemometrics. The quantum yields were low, with the highest reported being 1.53 +/- 0.41 %. However, this value fits in-between previously reported quantum yields for lanthanide-based luminescent nanomaterials (0.005-0.3 % and 4-16 %).[6,7]

The actual % Eu^{3+} doping amounts were higher than theoretical in all cases. This may be due to the microwave energy more directly interacting with Eu[EDTA] complexes than with Ca[EDTA] complexes, even though EDTA is known to bind more strongly to trivalent ions as opposed to divalent. The presence of europium was further confirmed through EDX.

While the crystalline purity was found to be very high, crystallite size as estimated using the Scherrer equation was smaller than the average particle size, signifying that each particle is made up of multiple crystallites. DLS measurements of EDTA-coated doped nanoparticle product show very high dispersion in aqeuous solutions, signifying viability in biological environments, but this dispersion appeared to be diminished by the presence of TTA on the surface of the nanoparticles. This was expected due to the hydrophobicity of the TTA molecule.

Future Work

Currently, there are two projects related to CaF_2 nanoparticles being carried out by undergraduate research students. The first of which is keeping the Eu^{3+} doping amount constant while varying the size of the nanoparticles. This is to discover the effect of particle size on the luminescent quantum yield. Another project concerns the doping of CaF_2 nanoparticles with Tb^{3+} and coating them with acetylacetonate (acac). Acetylacetonate is known to have efficient transitions of absorbed UV energy to Tb^{3+}.

The TTA coating procedure needs to be more thoroughly explored. Past projects have shown some % Eu^{3+} doping amounts to have higher quantum yields with lower concentrations of TTA, while others have been shown to have higher quantum yields with higher concentrations of TTA.

Work moving this nanoparticle system towards a biological application also needs to be completed. *In vitro* imaging with TTA-coated Eu:CaF_2 nanoparticle product using an epifluorescence microscope is the first step that can be completed here at Western Carolina University.

REFERENCES

[1] Xia, Y. Nanomaterials at work in biomedical research. *Nature materials* **2008**, *7*, 758.

[2] Xie, J.; Lee, S.; Chen, X. Nanoparticle-based theranostic agents. *Advanced drug delivery reviews* **2010**, *62*, 1064–1079.

[3] Peng, H.-S.; Chiu, D. T. Soft fluorescent nanomaterials for biological and biomedical imaging. *Chemical Society Reviews* **2015**, *44*, 4699–4722.

[4] Shi, J.; Sun, X.; Li, J.; Man, H.; Shen, J.; Yu, Y.; Zhang, H. Multifunctional near infrared-emitting long-persistence luminescent nanoprobes for drug delivery and targeted tumor imaging. *Biomaterials* **2015**, *37*, 260–270.

[5] Hagan, A.; Zuchner, T. Lanthanide-based time-resolved luminescence immunoassays. *Analytical and bioanalytical chemistry* **2011**, *400*, 2847–2864.

[6] Boyer, J.-C.; Van Veggel, F. C. Absolute quantum yield measurements of colloidal NaYF 4: Er3+, Yb3+ upconverting nanoparticles. *Nanoscale* **2010**, *2*, 1417–1419.

[7] Runowski, M.; Lis, S. Preparation and photophysical properties of luminescent nanoparticles based on lanthanide doped fluorides (LaF3: Ce3+, Gd3+, Eu3+), obtained in the presence of different surfactants. *Journal of Alloys and Compounds* **2014**, *597*, 63–71.

[8] Bünzli, J.-C. G.; Piguet, C. Taking advantage of luminescent lanthanide ions. *Chemical Society Reviews* **2005**, *34*, 1048–1077.

[9] Li, Z.; Zhang, Y.; Huang, L.; Yang, Y.; Zhao, Y.; El-Banna, G.; Han, G. Nanoscale fluorescent stone: luminescent calcium fluoride nanoparticles as theranostic platforms. *Theranostics* **2016**, *6*, 2380.

[10] Safronikhin, A.; Ehrlich, H.; Lisichkin, G. Double-jet precipitation synthesis of CaF2 nanoparticles: The effect of temperature, solvent, and stabilizer on size and morphology. *Journal of Alloys and Compounds* **2017**, *694*, 1182–1188.

[11] Sharma, G.; Narula, A. K. Eu 3+-doped CaF 2 nanoparticles functionalized by salicylic acid: synthesis, structural, optical and morphological studies. *Journal of Materials Science: Materials in Electronics* **2016**, *27*, 4928–4934.

[12] Wang, F.; Fan, X.; Pi, D.; Wang, M. Synthesis and luminescence behavior of Eu3+-doped CaF2 nanoparticles. *Solid state communications* **2005**, *133*, 775–779.

[13] Zhao, L.; Kutikov, A.; Shen, J.; Duan, C.; Song, J.; Han, G. Stem cell labeling using polyethylenimine conjugated (α-NaYbF4: Tm3+)/CaF2 upconversion nanoparticles. *Theranostics* **2013**, *3*, 249.

[14] Zhang, C.; Li, C.; Peng, C.; Chai, R.; Huang, S.; Yang, D.; Cheng, Z.; Lin, J. Facile and controllable synthesis of monodisperse CaF2 and CaF2: Ce3+/Tb3+ hollow spheres as efficient luminescent materials and smart drug carriers. *Chemistry–A European Journal* **2010**, *16*, 5672–5680.

[15] De Silva, C. R.; Maeyer, J. R.; Wang, R.; Nichol, G. S.; Zheng, Z. Adducts of europium β-diketonates with nitrogen p, p-disubstituted bipyridine and phenanthroline ligands: Synthesis, structural characterization, and luminescence studies. *Inorganica chimica acta* **2007**, *360*, 3543–3552.

[16] Ma, L.; Yang, L.-L.; Wang, Y.-G.; Zhou, X.-P.; Xu, X.-Y. Microwave-assisted preparation of nearly monodisperse flower-like CaF2 microspheres. *Ceramics International* **2013**, *5*, 5973–5977.

[17] Gerbec, J. A.; Magana, D.; Washington, A.; Strouse, G. F. Microwave-enhanced reaction

rates for nanoparticle synthesis. *Journal of the American Chemical Society* **2005**, *127*, 15791–15800.

[18] Williamson, C. B.; Nevers, D. R.; Hanrath, T.; Robinson, R. D. Prodigious effects of concentration intensification on nanoparticle synthesis: a high-quality, scalable approach. *Journal of the American Chemical Society* **2015**, *137*, 15843–15851.

[19] Chithrani, B. D.; Ghazani, A. A.; Chan, W. C. Determining the size and shape dependence of gold nanoparticle uptake into mammalian cells. *Nano letters* **2006**, *6*, 662–668.

[20] Muniz, F. T. L.; Miranda, M. R.; Morilla dos Santos, C.; Sasaki, J. M. The Scherrer equation and the dynamical theory of X-ray diffraction. *Acta Crystallographica Section A: Foundations and Advances* **2016**, *72*, 385–390.

[21] Singh, A. K. *Advanced x-ray techniques in research and industry*; IOS Press, 2005.

[22] Shi, M.; Li, F.; Yi, T.; Zhang, D.; Hu, H.; Huang, C. Tuning the triplet energy levels of pyrazolone ligands to match the 5D0 level of europium (III). *Inorganic chemistry* **2005**, *44*, 8929–8936.

[23] Magde, D.; Brannon, J. H.; Cremers, T. L.; Olmsted, J. Absolute luminescence yield of cresyl violet. A standard for the red. *Journal of Physical Chemistry* **1979**, *83*, 696–699.

[24] Goncalves e Silva, F. R.; Malta, O. L.; Reinhard, C.; Güdel, H.-U.; Piguet, C.; Moser, J. E.; Bünzli, J.-C. G. Visible and near-infrared luminescence of lanthanide-containing dimetallic triple-stranded helicates: energy transfer mechanisms in the SmIII and YbIII molecular edifices. *The Journal of Physical Chemistry A* **2002**, *106*, 1670–1677.

[25] Faulkner, S.; Pope, S. J.; Burton-Pye, B. P. Lanthanide complexes for luminescence imaging applications. *Applied Spectroscopy Reviews* **2005**, *40*, 1–31.

[26] Brennetot, R.; Georges, J. Investigation of chelate formation, intramolecular energy transfer and luminescence efficiency and lifetimes in the Eu–thenoyltrifluoroacetone–trioctylphosphine oxide–Triton X-100 system using absorbance, fluorescence and photothermal measurements. *Spectrochimica Acta Part A: Molecular and Biomolecular Spectroscopy* **2000**, *56*, 703–715.

[27] Tibi, M.; Heumann, K. G. Multi-element trace determinations in pure alkaline earth fluoride powders by high-resolution ICP-MS using wet-chemical sample preparation and laser ablation. *Analytical and bioanalytical chemistry* **2003**, *377*, 126–131.

[28] Gorry, P. A. General least-squares smoothing and differentiation by the convolution (Savitzky-Golay) method. *Analytical Chemistry* **1990**, *62*, 570–573.

[29] Alharbi, N. D. Size controlled CaF 2 nanocubes and their dosimetric properties using photoluminescence technique. *Journal of Nanomaterials* **2015**, *16*, 302.

[30] Yang, Z.; Wang, G.; Guo, Y.; Kang, F.; Huang, Y.; Bo, D. Microwave-assisted synthesis and characterization of hierarchically structured calcium fluoride. *Materials Research Bulletin* **2012**, *47*, 3965–3970.

[31] Azami, M.; Jalilifiroozinezhad, S.; Mozafari, M.; Rabiee, M. Synthesis and solubility of calcium fluoride/hydroxy-fluorapatite nanocrystals for dental applications. *Ceramics international* **2011**, *37*, 2007–2014.